ACS Biomaterials SCIENCE & ENGINEERING

pubs.acs.org/journal/abseba

Article

Liquid CO_2 Formulated Mesoporous Silica Nanoparticles for pH-Responsive Oral Delivery of Meropenem

Aun Raza, Fekade Bruck Sime, Peter J. Cabot, Jason A. Roberts, James R. Falconer,* Tushar Kumeria,* and Amirali Popat*

Cite This: *ACS Biomater. Sci. Eng.* 2021, 7, 1836–1853

Read Online

ACCESS | Metrics & More | Article Recommendations | Supporting Information

ABSTRACT: Meropenem (MER) is an effective broad-spectrum antibiotic currently only available in the parenteral form requiring frequent drug preparation and administration due to its extremely poor stability. The unavailability of oral Meropenem is primarily due to its ultrapoor handling and processing stability, hydrophilic nature that inhibits the passive diffusion across the gastrointestinal (GI) epithelium, degradation in the harsh gastric environment, and GI expulsion through enterocyte efflux glycoproteins. In this regard, we have developed an oral drug delivery system that confines MER into mesoporous silica nanoparticles (MSNs i.e, MCM-41 ∼141 nm) using a novel liquid carbon dioxide (CO_2) method. MER was efficiently encapsulated within pristine, phosphonate (negatively charged MSN), and amine (positively charged MSN) modified MSNs with loading capacity ranging between 25 *wt* % and 31 *wt* %. Next, the MER-MCM-NH_2 particles were electrostatically coated with Eudragit S100 enteric polymer that protected MER against gastric pH (pH 1.9) and enabled site-specific delivery in the small intestine (pH 6.8). Cellular uptake results in RAW 264.7 macrophage, Caco-2, and LS174T cells confirming the efficient cellular uptake of nanoparticles in all three cell lines. More importantly, the bidirectional transport (absorptive and secretory) of MER across Caco-2 monolayer was significantly improved for both MSN-based formulations, particularly MSNs coated with a polymer (Eud-MER-MCM-NH_2) where permeability was significantly enhanced (∼2.4-fold) for absorptive transport and significantly reduced (∼1.8-fold) for secretory transport. Finally, *in vitro* antibacterial activity [minimum inhibitory concentration (MIC)] and time-kill assay against *S. aureus* and *P. aeruginosa* showed that drug-loaded nanoparticles were able to retain antibacterial activity comparable to that of free MER in a solution at equivalent dose. Thus, Eudragit-coated silica nanoparticles could offer a promising and novel solution for oral delivery of Meropenem and other such drugs.

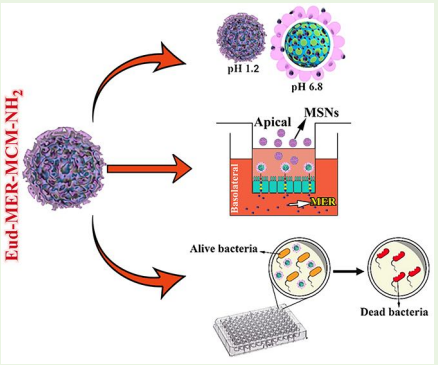

KEYWORDS: *liquid CO_2, Meropenem, oral antibiotics, mesoporous silica nanoparticles, oral drug delivery*

1. INTRODUCTION

Antimicrobial resistance (AMR) is a major threat to global health because increasing infectious pathogens are developing resistance to known antimicrobial agents. It is predicted that antibiotic-resistant pathogens will affect nearly 230 million people every year by 2050 and cumulatively cost the US $100 trillion to the world economy between 2014 and 2050. At present, globally, around 700,000 people die each year due to infections caused by antibiotic-resistant pathogens, and this is predicted to reach 10 million people by 2050.[1] Therefore, the discovery of new antibiotics for a range of pathogens is a priority of the global healthcare industry and supported by the World Health Organization (WHO). However, the drug discovery process is excessively expansive and enormously time-consuming. In this regard, advanced formulation approaches to improve the efficacy of existing antibiotics to reduce AMR are considerably cheaper and quicker.[2] Advanced formulation approaches reduce AMR development by improving key properties of current antibiotics including molecular instability, low bacterial uptake, and low permeability resulting in poor bioavailability.[3]

The carbapenem family of antibiotics that include Meropenem, imipenem, and others are structurally related to β-lactam antibiotics (penicillin and cephalosporin) and considered unique because of their resistance against extended-spectrum beta-lactamases (ESBLs). Meropenem (MER) is *slightly soluble* (5.63 mg/mL) *in water with* a logP value of −0.6.[4,5] MER has excellent bactericidal activity against Gram-positive and Gram-negative bacteria.[6,7] The mode of action of MER is inhibition of bacterial cell wall synthesis like other beta-lactams; however, MER is more resistant to

Special Issue: Nanomedicine Advances in Infectious Diseases

Received: August 31, 2020
Accepted: December 23, 2020
Published: January 7, 2021

https://dx.doi.org/10.1021/acsbiomaterials.0c01284
ACS Biomater. Sci. Eng. 2021, 7, 1836–1853

Scheme 1. Schematic Summary of the Preparation of the Liquid CO_2 Processed Eud-MER-MCM-NH_2 Formulation and Their Systematic Testing[a]

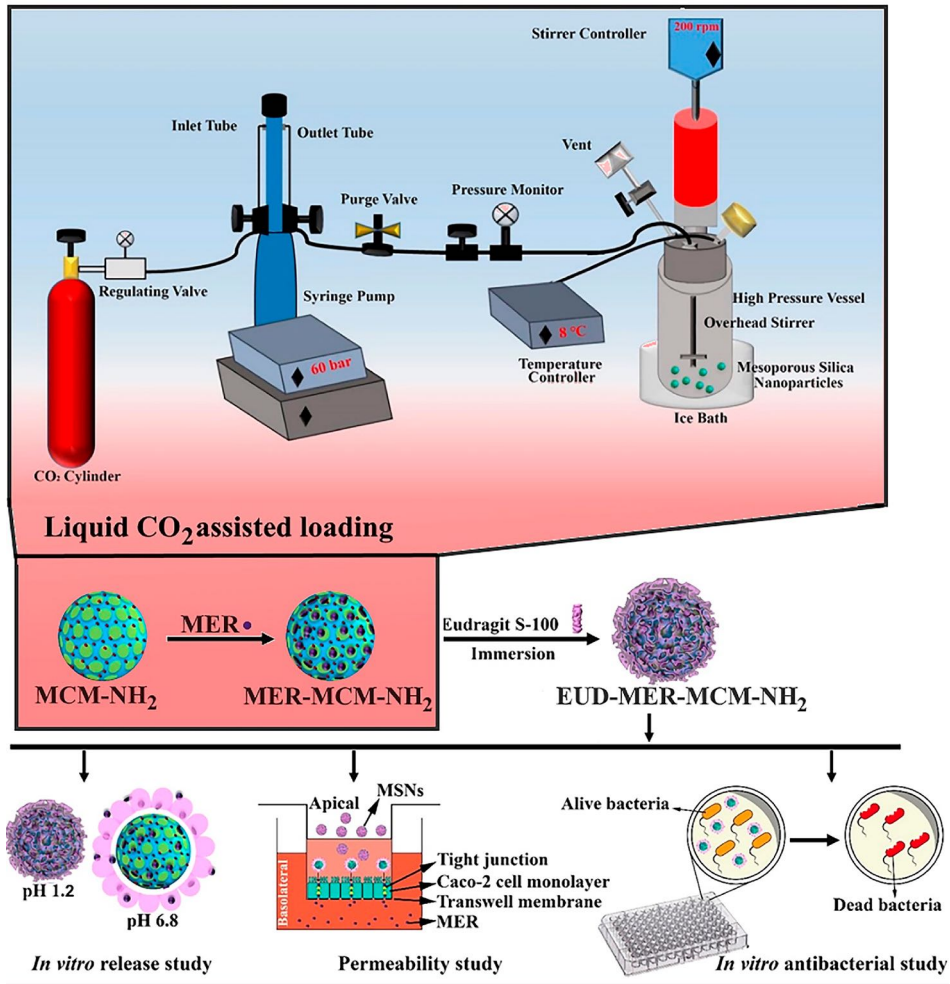

[a]First, MER was loaded into MCM-41 nanoparticles using a novel liquid CO_2 process as outlined in the top section of the scheme. The setup includes a high-pressure stainless-steel vessel maintained at a pressure of 60 bar using a syringe pump. The temperature of the vessel is maintained between 6-8 °C using an ice-bath, and the overhead stirrer rotating at 200 rpm ensures homogenous loading of MER into MCM-41 nanoparticles. After loading MER into MCM, Eudragit S100 was coated to achieve pH-responsive release. Later, MER permeability studies were carried out using a Caco-2 monolayer culture model to analyze the transport of MER across the intestinal barrier. Lastly, the efficacy of the prepared oral MER formulations was carried out against *P. aeruginosa* and *S. aureus* using antibacterial assays.

degradation caused by beta-lactamases.[8] It also lacks susceptibility to dehydropeptidase-1 (DHP-1), which hydrolyzes other carbapenems, and exhibits superior activity against *Pseudomonas aeruginosa* and all *Enterobacteria* compared to other carbapenems; thus, it is known as a broad-spectrum antibiotic.[9,10] Therefore, the heterogeneous activity of MER makes it an ideal candidate to work against serious infections caused by drug-resistant bacteria.[11]

Currently, MER is administered parentally via intermittent bolus infusion or continuous infusion to minimize the drug degradation in aqueous solution over time and to achieve maximum therapeutic drug concentration in patients to treat infections, respectively.[12] However, intermittent bolus infusion results in drug concentration falling below the minimum inhibitory concentration (MIC).[11,12] Further, short circulation half-life and fluctuation in plasma concentrations of MER are the possible reasons for its frequent high doses of 0.5−2 g thrice a day. Patients, even with normal renal functions, showed extremely low plasma protein binding (2%) and short elimination half-life of 1 h.[13] It is also investigated that approximately 70% of MER dose is excreted from the kidney in unchanged form after 12 h, and 28% is recovered as inactive metabolites.[14] Moreover, continuous infusion of Meropenem demands frequent drug preparation and administration due to its short stability in an aqueous solution. MER undergoes hydrolysis, which results in the opening of the β-lactam ring to produce degradation products, which could cause anaphylactic reaction and loss of antibacterial activity.[8,15,16]

A study by Fawaz et al. illustrated that Meropenem could be continuously administered to patients for at least 7 or 5 h at 22 or 33 °C, respectively.[16] Also, solid-state stability studies showed that carbapenems such as MER and tebipenem are also unstable at 40 °C after 5 h and undergo thermolysis, which could also produce toxic degradation products.[17,18] Because of the low thermal stability, intermittent bolus administration is preferred, which requires frequent drug preparation by a registered pharmacist and intermittent dose administration by a nurse. MER dosage compounding in hospitals without

https://dx.doi.org/10.1021/acsbiomaterials.0c01284
ACS Biomater. Sci. Eng. 2021, 7, 1836−1853

temperature monitoring systems can lead to suboptimal MER dose administration with compromised activity.[19] Also, after successful MER (IV) administration, once the health of the patient improves, switching to oral treatment has multiple advantages, including short inpatient admission with lower nursing cost and increased patient compliance. Therefore, developing oral formulations of antimicrobials such as MER is urgently warranted.

Unfortunately, MER suffers from poor oral bioavailability due to its hydrophilicity—inhibiting the passive diffusion across the GI epithelium, instability in the gastric environment, and GI expulsion through enterocyte efflux glycoproteins (MDR1, ABCB1).[20] One strategy to improve the poor oral bioavailability and chemical stability of carbapenems is to design MER prodrugs. Prodrugs of Meropenem and other carbapenems such as ertapenem and tebipenem have been developed and show improved bioavailability without losing their antibacterial effects.[21,22] Currently, available MER prodrugs are susceptible to acid—base hydrolysis and produce large amounts of toxic metabolites during this process, while the thermolysis of the drug in the solid-state remains a problem.[23,24] Consequently, the cost associated with these prodrug development and long regulatory approval processes makes prodrug development financially nonviable.

Encapsulation of drugs into nanoparticle has proven to be a promising way to improve the therapeutic efficacy of many drugs including antibacterial agents.[26−28] Recently, many new formulation approaches have been used for targeted oral drug delivery. Among these, polymer—lipid hybrid systems, mucoadhesive dendrimers, lipid-based delivery systems (nanoemulsions, nanostructured lipid carriers, and solid lipid nanoparticles), polymeric systems, and miscellaneous nanocarriers (nanocrystals, carbon nanotubes, and metallic nanocarriers) are mostly used to achieve targeted oral drug delivery via improving solubility and dissolution of hydrophobic drugs.[25] Different types of nanocarriers are commonly used for oral antimicrobial drug delivery such as polymeric and lipid nanocarrier (solid lipid nanoparticles, liposomes, and polymeric micelles, etc.) and inorganic nanocarriers (i.e, mesoporous silica nanoparticles).[28,29] However, conventional nanocarriers suffer from many disadvantages such as poor loading capacity (especially important for high dose antibiotics), poor stability, and complex manufacturing methods.

Previously, MER loaded liposomes,[29] synthetic polymeric nanoparticles,[30,31] and lipid-based nanocarriers[32] have been reported. However, high cost, low drug encapsulation efficiency (e.g., 3.7−7.2% for liposomal-MER[29]) and loading capacity (e.g., 3−4% for MER-loaded poly(ε-caprolactone[30]), low shelf-lifetime, instability (e.g., liposomes are highly liable to gastric acid, bile salts, and enzymes, while polymer-based systems are unstable in water), and premature drug release are key issues associated with these carriers.[29,31,32] To overcome these limitations, mesoporous silica nanoparticles (MSNs) (MCM-41, MCM-48, and SBA-15) appear as promising candidates for oral drug delivery.[33−42] Several advantages of MSNs, such as easy synthesis procedure, tunable pore and particle sizes, efficient and simple functionalization, high surface area (>1000 m^2/g), and large pore volume adequate for high drug loading, make them appropriate candidates for oral delivery of MER.[43] Moreover, MSNs have been shown to enhance the stability of drugs in the GI tract, improve thermostability, and enhance oral bioavailability and therapeutic efficacy of both hydrophilic and hydrophobic drugs.[37,38,44] In addition, surface-functionalized MSNs could also provide high drug loading and slow drug release.[34,38] Due to the thermolability of MER, the conventional method of drug loading such as the solvent evaporation method, immersion method (high temperature), and hot-melt extrusion are not suitable. To achieve bioactive MER loading into MCM-41, an effective new method is required. Supercritical CO_2 ($scCO_2$) and liquid CO_2 usually work at mild conditions (low temperature and pressure) and are widely used for the extraction of thermolabile compounds.[45] Moreover, CO_2 is cost-effective, nontoxic, and nonflammable and is recognized as a safe solvent by the US-FDA, relative to commonly used organic solvents used in pharmaceutical processing, and does not require the multistep process of conventional methods (drying and grinding/milling, etc.).[46,47] Therefore, $scCO_2$ and liquid CO_2 have been successfully used as an alternative to conventional methods for drug loading into different nanocarriers including polymeric, lipid, and inorganic (e.g., MSNs).[46,48,49]

In this study, liquid CO_2 was used for the first time to load MER into functionalized MCM-41 nanoparticles to achieve ultrahigh drug loading capacity (Scheme 1, top) and coated with Eudragit S100 enteric polymer to develop a novel pH-sensitive oral formulation of MER (Scheme 1, bottom). Eudragit S100 coating performs a multifaceted role in this formulation by protecting MER from gastric pH, enables targeted delivery in the small intestine and colon, and enhances the intestinal permeation.[50,51] Using this unique green technique, we achieved close to 25 *wt* % MER loading capacity which is considerably higher compared to previously reported MER formulations.[29,30] The presented novel formulation showed no drug release at gastric pH and controlled-release at small intestinal pH after coating. Furthermore, amine-modified MSNs with Eudragit S-100 coating were taken up by both macrophages (RAW 264.7) and intestinal epithelial cancer cells (LS 174T and Caco-2), demonstrating the potential of this system to deliver MER intracellularly. Finally, we demonstrated that coated MSNs could improve the permeability of MER while retaining its antibacterial effects.

2. MATERIALS AND METHODS

2.1. Materials. Cetyltrimethylammonium bromide (CTAB), tetraethyl orthosilicate (TEOS), (3-aminopropyl) triethoxysilane (APTES), 3-(trihydroxy silyl) propyl methyl phosphonate (THMP), dimethyl sulfoxide (DMSO), glacial acetic acid (CH_3COOH), and toluene were purchased from MERK, Frenchs Forest, Australia. Sodium hydroxide (NaOH), phosphoric acid (H_3PO_4), hydrochloric acid (HCl, 32% w/w), acetonitrile (HPLC grade), dichloromethane (DCM), and dipotassium hydrogen orthophosphate anhydrous were purchased from Chem-Supply (Gillman, SA, Australia). Meropenem trihydrate of analytical standard ≥98% (Fujifilm Wako Pure Chemical Corporation, China) was used. MTT (3-(4,5-dimethyl-2-thiazolyl)-2,5-diphenyl-2H-tetrazolium bromide) reagent and cyanine5 NHS ester (Cy-5) were purchased from Tocris Bioscience, Australia. Dulbecco's modified eagle medium (DMEM) with phenol red (D6556 and D5796) and without phenol red (D8537), Dulbecco's phosphate-buffered saline (PBS), fetal bovine serum (FBS), Triton X-100, paraformaldehyde, MEM nonessential amino acid solution (100X), phalloidin-FITC (fluorescein isothiocyanate), and DAPI (4′,6-diamidino-2-phenylindole) were purchased from Sigma-Aldrich, Australia. Pen-Strep (Penicillin 10,000 U/mL and Streptomycin 10,000 μg/mL), Hank's balanced salt solution (HBSS), 0.25% Trypsin-EDTA (1X), L-glutamine (100X), and sodium pyruvate (100 mM) from Gibco; Thermo Fisher Scientific, Australia. A liquid

https://dx.doi.org/10.1021/acsbiomaterials.0c01284
ACS Biomater. Sci. Eng. 2021, 7, 1836−1853

Scheme 2. Schematic Illustration for Surface Functionalization of MCM-41 with (a) Silane with an Amine Terminal (Aminopropyl Triethoxysilane; APTES) and (b) Silane with Phosphonate Terminal (3-(trihydroxy silyl) propyl methyl phosphonate; THMP)[a,b]

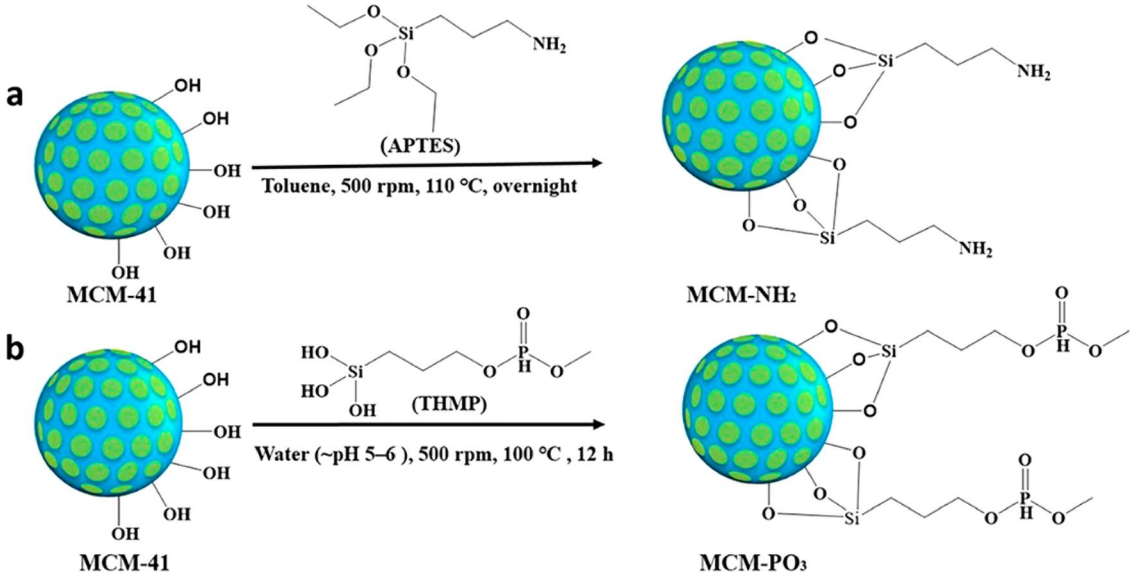

[a]The APTES was added dropwise into MCM-41 particles, and the reaction mixture was then refluxed overnight at 110 °C and stirred at 500 rpm. [b]MCM-41 particles dispersed in 20 mL of DI water using a bath sonicator for 3 min. THMP [3-(trihydroxysilyl)propylmethyl phosphonate] was added into another 45 mL of DI water, and the pH was adjusted to ~pH 5−6 to avoid hydroxylation and condensation of silanol groups on MCM-41 during the functionalization. This mixture was added into a particle dispersion, refluxed overnight at 100 °C, and stirred at 500 rpm.

CO_2 cylinder was purchased from BOC Australia. Ultrapure deionized water with a resistivity of 18 MΩ was (Millipore Milli-Q) used for the preparation of all the aqueous solutions.

2.2. Synthesis of MCM-41. MCM-41 particles were prepared by following the protocol of Abbarajuu et al. with slight changes.[52] Briefly, we measured out 480 mL of deionized (DI) water into a clean 1 L glass bottle with a magnetic stirrer in it and placed this glass bottle on a magnetic stir/heating ensemble. One gram of CTAB was weighed and dissolved completely (clear solution) in the glass bottle at 500 rpm and room temperature. Then, 2 M NaOH (3.5 mL) was added to the CTAB solution and the temperature of the oil bath was increased to 80 °C. Once at 80 °C, a Pasteur Pipette was used to add (slowly) 6.7 mL of TEOS straight into the eye of the whirlpool of the mixture. This mixture was stirred at 700 rpm for 2 h at 80 °C. The resulting suspension was then vacuum filtered and washed thrice with DI water. The filtrate was dried overnight in an oven at 60 °C. The dried filtrate was then crushed into a fine powder and added to the crucible. The crucible was placed in a muffle furnace, and filtrate was calcined at a maximum temperature of 550 °C over a 5 h period (It was slowly heated up to 550 °C in 2 h (5 °C/min) and then heated for 5 h at 550 °C and then slowly return (10 °C/min) to ambient temperature).

2.3. Surface Functionalization of MCM-41. Amino (NH_2) and phosphonate (PO_3) terminal functional groups were grafted onto the MCM-41 particles through well-established silane chemistry using the previously described methods with slight modification.[53,54] For NH_2 functionalization (Scheme 2a), MCM-41 particles (400 mg) were dispersed in 60 mL of toluene using a bath sonicator for 3 min and stirred (500 rpm) at 50 °C for 30 min. The APTES (0.4 mL) was then added dropwise, and the reaction mixture was then refluxed overnight at 110 °C and stirred at 500 rpm. MCM-NH_2 particles were separated from the reaction mixture by centrifugation at 14,000 rpm for 10 min. The MCM-NH_2 particles were washed twice with ethanol and once with water and dried overnight at 60 °C. For PO_3 functionalization (Scheme 2b), MCM-41 particles (400 mg) were dispersed in 20 mL of DI water using a bath sonicator for 3 min. THMP (0.4 mL) was added into another 45 mL of DI water, and the pH was adjusted to a value between 5−6 to avoid hydroxylation and condensation of silanol groups on MCM-41 during the functionalization. This mixture was added into the particle dispersion and refluxed overnight at 100 °C and stirred at 500 rpm. The functionalized particles were collected through centrifugation at 14,000 rpm for 10 min. These particles were then washed twice with acetone and once with water before drying overnight at 60 °C.

2.4. Loading of MER into MCM-41 Using Immersion and Liquid CO_2 Methods. MER was loaded into the pristine and functionalized MCM-41 particles using immersion and liquid CO_2 methods.

2.4.1. Immersion Method. To obtain 30% mass loading, MER (30 mg) and pristine or functionalized MCM-41 (70 mg) were added in 8 mL of water for the preparation of nanoparticles. The solution was magnetically stirred at 4 °C for 24 h. Drug loaded particles were freeze-dried overnight and stored at 4 °C.

2.4.2. Liquid CO_2 Method. A high-pressure stainless steel vessel (Nottingham, UK) (Scheme 1) was used to load MER into pristine or functionalized MCM-41 (i.e., MCM-NH_2 and MCM-PO_3). To obtain 30% mass loading, MER (30 mg) and pristine or functionalized MCM-41 (70 mg) were added into the vessel in the presence of 1 mL of water as cosolvent. After that, liquid CO_2 was pumped into the vessel using a syringe pump (Nottingham, UK) with a pressure of 60 bar. The vessel was placed in an ice bath to maintain its temperature at 6−8 °C. The stirring rate of 200 rpm was controlled using an overhead stirrer fitted in the vessel top. At the end of the experiment (4 h), the system was slowly depressurized, and this pressure drop was responsible to change liquid CO_2 into CO_2 gas, which was released back into the air. Loaded particles were later collected and stored at 4 °C until further analysis.

2.5. Cy-5 Grafting on MCM-NH_2. For covalent attachment of Cy-5 to aminated MCM, 30 mg of MCM-NH_2 was dispersed into 3 mL of DMSO and sonicated for 5 min. A solution of Cy-5 (3 mg/mL) was also prepared in DMSO. Then, 1 mL of Cy-5 solution was added into 3 mL of MCM-NH_2 and stirred (500 rpm) for 24 h at 4 °C. This reaction was covered with Al foil to protect Cy-5 from light. After 24 h, loaded particles were centrifuged at 10,000 rpm for 5 min and washed thrice with ethanol and water (3:1). Later, the pellet was

https://dx.doi.org/10.1021/acsbiomaterials.0c01284
ACS Biomater. Sci. Eng. 2021, 7, 1836−1853

vacuum-dried for 24 h, and dried loaded particles were stored at −20 °C in the dark.

2.6. Coating with Eudragit S100. For electrostatic enteric coating on MCM-NH_2, 30 mg of Eudragit S100 was dissolved into 3 mL of ethanol. Then 30 mg of MER-MCM-NH_2 orCy5-MCM-NH_2 was dispersed into 3 mL of the polymeric solution and stirred (500 rpm) for 4 h at 4 °C. The dispersed particles were centrifuged at 10,000 rpm for 5 min to collect nanoparticles which were washed thrice with ethanol and water (3:1) to remove the uncoated Eudragit S100, ungrafted Cy5, and MER that may have leached during the coating process. Nanoparticles obtained after centrifugation were freeze-dried for 24 h. Unloaded MCM-NH_2 nanoparticles (i.e., without MER) were also coated similarly and labeled as Eud-MCM-NH_2 for determining the amount of Eudragit S100 coated on nanoparticles using TGA. Dried coated particles (Eud-MCM-NH_2, Eud-MER-MCM-NH_2, and Eud-Cy5-MCM) were stored at 4 °C.

2.7. Characterization of Nanoparticles. TEM images of MSNs were acquired by an Hitachi 7700 (Hitachi, Japan) electron microscope at an acceleration voltage of 80 kV. Sample preparation for SEM was performed in a few steps, including (i) putting the carbon tapes on aluminum stubs, (ii) mounting the empty silicon wafers on carbon tapes, (iii) mounting samples on silicon wafers and labeling them at the back of the stubs, (iv) plasma cleaning (Evactron 25, Japan) of samples for 10 min, and (v) carbon coating [(*Quorum Q150-TES*, UK), 20 nm thickness))] of samples. For SEM images, a JEOL-JSM-7100F (Jeol, Japan) microscope was used at 10 kV that was fitted with an Energy-dispersive X-ray spectroscopy (EDXS) detector to perform elemental analysis of the samples.

Nitrogen adsorption Brunauer−Emmett−Teller (N_2-BET) (Tristar, Micromeritics-II, Norcross, GA, USA) was operated to measure the pore size, volume, and surface area of MSNs. The particle size and surface charge were calculated in water (solvent) by dynamic light scattering (DLS) and zeta potential measurements (Malvern, Nano-ZS, ATA Scientific, Taren Point, Australia). Thermogravimetric analysis (TGA) (Mettler Toledo, TGA/DSC 2, Columbus, OH, USA) was performed with a heating rate of 10 °C/min. X-ray diffractograms and wide-angle XRD were recorded using a Bruker X-ray diffractometer (*Bruker D8 Advance MKII* XRD, Germany) with Cu radiation (λ = 1.54 Å). MER concentrations were determined using the UHPLC (Agilent 1290 Infinity, USA) method based on existing literature with slight modification.[55] Dipotassium hydrogen orthophosphate buffer (30 mM) was prepared in distilled water, and the pH was adjusted to 3 by orthophosphoric acid. A Kinetex C18 column was used (LC 250 × 4.6 mm, 5 μm (Phenomenex, USA) for quantification analysis. MER was eluted isocratically with mobile phase [acetonitrile (A)/30 mM phosphate buffer (B) at the ratio of 10/90%] at a flow rate of 0.7 mL/min, column temperature of 10 °C, and 10 μL injection volume and monitored with a UV detector at 220 nm. The concentration of MER was calculated using a standard calibration curve with a linear regression fitting factor (R^2) of 0.999.

2.8. *In Vitro* Release Study. First, we investigated the effect of simulated gastric fluid (pH 1.2) and simulated intestinal fluid (pH 6.8) with enzymes [United States Pharmacopeia (USP)][56] on the stability of MER. After that, MCM-MER, MCM-PO_3-MER, and MCM-NH_2-MER (800 μg equivalent MER) were dispersed in 5 mL of simulated gastric fluid (pH 1.2) and simulated intestinal fluid (pH 6.8) without enzymes [United States Pharmacopeia (USP)][56] and stirred at 100 rpm and 37 °C. Aliquots (0.2 mL) were taken at 0.25, 0.5, 1, 1.5, 2, 4, 6, and 8 h and centrifuged at 14,000 rpm for 4 min. An equal volume of fresh buffers (pH 1.2 and 6.8) was added to rinse the pellet and put back the suspension to the total volume of release buffer. However, the pH-dependent release of MER from MER-MCM-NH_2 with Eudragit S100 coating was investigated using a "universal" buffer. Aqueous solutions of 0.05 M H_3PO_4 and 0.05 M CH_3COOH were mixed in a 1:1 (v/v) ratio to form a solution with a pH of 1.2. This solution was titrated at defined time points during the release experiment using 8 M NaOH to produce buffers with a pH of 6.8. Eud-MER-MCM-NH_2 (765 μg MER equivalent) was dispersed into 5 mL of universal buffer (5 mL of the universal buffer with pH 1.2 contained 2.5 mL of 0.05 M H_3PO_4 and 2.5 mL of 0.05 M CH_3COOH) and stirred at 100 rpm at 37 °C under sink conditions. After 2 h, the pH was titrated to pH 6.8 by adding 25 μL of aqueous 8 M NaOH. Samples (200 μL) were withdrawn at predetermined time intervals and immediately replaced with an equal volume of fresh buffer solution of equivalent pH to maintain a constant volume. The withdrawn samples were centrifuged (14,000 rpm for 4 min) and run in UHPLC. The calculation of MER released from MSNs was quantified with reference to a standard curve.

2.9. *In Vitro* Biocompatibility of MCM-NH_2 and Eud-MCM-NH_2. MCM-NH_2 and Eud-MCM-NH_2 were tested for their potential cytotoxic effect on RAW 264.7 macrophages (ATCC) and intestinal epithelial cancer cells [(Caco-2 and LS174T cells), ATCC] using the MTT assay. RAW 264.7 macrophages and LS174T cells were cultured in DMEM medium (D6546), containing 1% each of pen-strep and L-glutamine and 10% FBS. Caco-2 cells were cultured using DMEM (D5796) with 1% v/v each of sodium pyruvate, pen-strep, L-glutamine, MEM nonessential amino acids, and 10% FBS. The cells were grown at 37 °C in a humidified incubator with 5% CO_2. RAW 264.7 macrophages (1.5×10^4 cells/well), Caco-2 cells (2×10^4 cells/well), and LS 174T cells (2×10^4 cells/well) were seeded into 96-well plates and grown for 24 h. The weighed masses of MCM-NH_2 and Eud-MCM-NH_2 were adjusted to give equivalent concentrations of 25, 50, 100, 250, 500, and 1000 μg/mL of silica in media and incubated with cells for 24 h. Cells with medium only were used as negative controls, and cells with solubilizing buffer (10% SDS in 0.1 N HCl) were used as positive controls for each plate. After incubation (24 h), the cell culture medium (with nanoparticles) was then aspirated and 100 μL/well of MTT reagent (0.5 mg/mL in PBS) was added for a further 4 h incubation at 37 °C. The formazan crystals were dissolved by adding 100 μL/well DMSO. The absorbance signal of formazan was measured at 570 nm using a microplate reader. Three independent experiments (n = 3) were conducted with triplicate wells per treatment for each cell line and concentration.

2.10. Cellular Uptake of Silica Nanoparticles. *2.10.1. Visualization of Cellular Uptake Using Laser Scanning Confocal Microscopy.* RAW 264.7 macrophage (2×10^5 cells/well), Caco-2 (2×10^5 cells/well), and LS 174T (2×10^5 cells/well) cells were seeded into a Cellvis glass-bottom dish (35 mm) and grown for 24 h. Eud-Cy5-MCM (100 μg/mL) prepared in the medium was added to the dish and incubated for 4 h at 37 °C. Cells with medium only were used as control. After 4 h of incubation, the medium was removed, and the cells were washed thrice with chilled PBS (pH 7.4). Afterward, the cells were fixed with chilled 4% paraformaldehyde at room temperature for 20 min and washed thrice with chilled PBS with gentle rocking. Then cells were permeabilized with 0.2% Triton X-100 in PBS for 30 min and washed thrice with chilled PBS with gentle rocking. To block nonspecific binding, cells were treated overnight with 1% BSA in PBS (2 mL) at 4 °C and then the cells were washed once with PBS. Subsequently, the filamentous actin cytoskeleton of cells was stained with 1 mL of Phalloidin-FITC (stock concentration 50 mg/mL, then 1 μL from the stock into 1 mL of PBS for staining) for 20 min and washed thrice with chilled PBS to remove excess dye. Then 0.5 mL of DAPI (stock concentration 5 mg/mL, then 1 μL from stock into 1 mL of PBS for staining)) was used for nuclei staining for 10 min and cells were then washed three times with chilled PBS to remove excess DAPI. Before imaging, PBS was added to avoid dehydrating the samples and the dish was covered with Al-foil to protect the stains from light. Cell imaging was performed using a laser scanning confocal microscope Olympus FV3000 with a 60× objective lens immersed in oil. Phalloidin-FITC was used to label the cytoskeleton of the cell ($\lambda_{ex\text{-}em}$ 496−516 nm; green), and DAPI was used to label the cell nuclei ($\lambda_{ex\text{-}em}$ 358−461 nm; blue). The Cy-5 signals were recorded at $\lambda_{ex\text{-}em}$ 646−670 nm (red).

2.10.2. Quantitative Assay of Cellular Uptake Using Flow Cytometry. RAW 264.7 macrophage (2×10^5 cells/well), Caco-2 (2×10^5 cells/well), and LS174T (2×10^5 cells/well) cells were seeded into 6-well plates and grown for 24 h. Cells were incubated with Eud-Cy5-MCM (100 μg/mL) for 2 h. Cells with medium only were used as control. After 2 h, all samples were washed five times with PBS to remove excess nanoparticles and then trypsinized,

https://dx.doi.org/10.1021/acsbiomaterials.0c01284
ACS Biomater. Sci. Eng. 2021, 7, 1836−1853

harvested, and suspended in 1 mL of PBS to measure the fluorescence intensity using a BD Accuri C6 flow cytometer, and data were analyzed using FlowJo FJXv10.0.8 software. To separate the debris population from a cell population, gating was done on the scattering gate (forward scattering: FSC-A; side scattering: SSC-A). To exclude a doublet, a single gate was adjusted using both SSC-W and FSC-W as well as SSC-H and FSC-H. To detect fluorescence related to Cy-5 dye ($\lambda_{ex\text{-}em}$ 646−670 nm), we used an FL4 detector.

2.10.3. Cellular Uptake of Silica Nanoparticles Studied Using TEM and STEM/EDXS. RAW 264.7 macrophages (3×10^5 cells/well) and LS174T cells (3×10^5 cells/well) were seeded in a 6 well plate (*Corning Costar* Corp, NY, USA) and grown for 24 h. To determine intracellular location, Eud-MCM-NH_2 was added into each well and incubated for 30 min (50 μg/mL) with both RAW 264.7 macrophages and LS174T cells or 3 h (100 μg/mL) with LS174T cells only. The sample was washed thrice with PBS to remove nanoparticles in the extracellular environment. The sample was fixed with 2.5% (v/v) glutaraldehyde in PBS and then postfixed with 2% (w/v) osmium tetroxide and 1.5% (w/v) potassium ferricyanide for 1 h. The sample was treated with 1% (w/v) thiocarbohydrazide for 20 min, 2% (w/v) osmium tetroxide for 30 min, 1% (w/v) uranyl acetate overnight at 4 °C, and lead aspartate for 1 h at 60 °C. Between each of these steps, the samples were washed three times with type 1 ultrapure water. Then, a graded series of EtOH solutions was used to dehydrate the sample for 5 min in each step. The sample was then embedded in Durcupan resin, and ultrathin sections were cut on a Leica Ultracut 6 ultramicrotome. Sections were viewed using a HITACHI HT7700 TEM. Scanning transmission electron microscopy with energy-dispersive X-ray spectroscopy (STEM/EDXS) analysis was conducted on these same sections using an HF5000TEM instrument.

2.11. *In Vitro* Caco-2 Permeability Experiments. The *in vitro* permeability of MER was determined using the Caco-2 cell monolayer assay. Caco-2 cells (passage number P-26) were cultured in Phenol red-free DMEM medium (D8537) with 1% v/v each of sodium pyruvate, pen-strep, L-glutamine, MEM nonessential amino acids, and 10% of FBS and incubated under 37 °C with 5% CO_2. When 90% confluency was reached, cells were trypsinized, harvested, and adjusted to a cell density of 2×10^5/mL using fresh DMEM medium. Then, a 0.5 mL cell suspension (1×10^5/mL) was seeded into the apical chamber (A) of 12 trans-well inserts (0.4 μm pore diameter, 1.12 cm^2 area) (Corning Inc., Kennebunk, ME, USA) plates. However, 1.5 mL of fresh medium was added into the basolateral chamber (B) of each insert.

2.11.1. Determination of TEER. First, the electrode of the EVOM volt-ohmmeter (World Precision Instruments, Sarasota, FL, USA) was pre-equilibrated in DMEM for 20 min. Meanwhile, the medium was changed from the transwell every second day, and 0.5 and 1.5 mL of fresh DMEM (preheated at 37 °C) were added to each well in A and B, respectively. After equilibrated at 37 °C for 20 min, Transepithelial Electrical Resistance (TEER) values were recorded. As a criterion, a monolayer with a Transepithelial Electrical Resistance (TEER) value ≥500 Ω·cm^2 was used for transport experiments.[57] The TEER values of Caco-2 monolayers was measured and calculated as the equation below

$$\text{TEER}\ (\Omega\cdot\text{cm}^2) = [\text{TEER}\ (\Omega) - \text{TEER}_{\text{background}}\ (\Omega)] \times \text{A}\ (\text{cm}^2) \quad (1)$$

TEER (Ω) is the electrical resistance across Caco-2 monolayers, $\text{TEER}_{\text{background}}$ (Ω) is the resistance across the insert only without cells. A (cm^2) is the surface area of the insert, 1.12 cm^2.

2.11.2. Bidirectional Transport Experiment. In our experiment, Caco-2 cells with TEER ≥ 500 Ω·cm^2 were recorded within 6 days, which is an indicator of monolayer development. To investigate the permeability (A to B), the medium from each well was replaced with preheated HBSS and equilibrated at 37 °C for 20 min. After that, the dosing (A) chamber was replaced with 200 μg/mL of MER alone or an equivalent concentration of MER-MCM-NH_2 and Eud-MER-MCM-NH_2 in HBSS and 1.5 mL of HBBS only in receiving chamber (B). Efflux study (B to A) was performed similarly; however, the dosing and receiving sides were B and A, respectively. Plates were placed in a shaking incubator (John Morris Scientific, Australia) at 37 °C and 100 rpm to simulate the small intestine motility. In each study, samples (0.2 mL) were taken out from the receiving chamber after 1 and 2 h. The volume of the receiving chamber was maintained constant by replacing the withdrawn samples with a similar volume of HBSS.

The apparent permeability coefficient (P_{app}, cm/s) was determined according to the following equation.

$$P_{app} = (dQ/dt)/(C_0 \times A) \quad (2)$$

dQ/dt is the MER transport rate (ng/s), C_0 is the initial concentration of MER on the dosing chamber (ng/mL). A is the surface area of inserts (1.12 cm^2).

The efflux ratio (ER) was determined using the following equation:

$$ER = P_{app}(B \rightarrow A)/P_{app}(A \rightarrow B) \quad (3)$$

$P_{app}(B \rightarrow A)$ and $P_{app}(A \rightarrow B)$ are representing the apparent permeability of tested formulations.

2.12. *In Vitro* Antibacterial Assay. *2.12.1. Broth Microdilution Method.* This method was used to determine the minimum inhibitory concentration (MIC_{90}) of antimicrobial agent that inhibits visible growth of a microorganism such as *P. aeruginosa* (ATCC 27853 and clinical strain 23) and *S. aureus* (ATCC 29213 and clinical strain 54) according to the procedure established by the European Committee on Antimicrobial Susceptibility Testing (EUCAST).[58,59] Briefly, serial 2-fold dilutions of antibiotic samples such as MER and MER nanoparticles (concentrations of MER in nanoparticles is equivalent ranged from 0.0313 mg/L to 16 mg/L) were prepared in CAMHB (cation adjusted Mueller Hinton Broth) and aliquoted (100 μL) into flat-bottom microtiter plates. McFarland 0.5 standardized inoculum suspension (1×10^6 CFU/mL) prepared in sterile distilled water was added into cation adjusted Mueller Hinton Broth (CAMHB) to give rise to approximately 1×10^6 CFU/mL. Then 100 μL of inoculum suspension prepared in CAMHB was added to the drug samples containing microtiter plates to give rise to approximately 5×10^5 CFU/mL. After that, inoculated plates were incubated at 37 °C for 16 to 20 h and MIC values were determined spectrophotometrically at 620 nm. This experiment for the determination of MIC values was repeated three times.

2.12.2. Static Time-Kill Studies. Static time-kill studies were performed to compare the pharmacodynamics (PD) activity of MER with its nanoformulations. Bacterial growth in antibiotic media was compared to a control, unexposed bacteria, to describe the activity of the antibiotic. Briefly, 200 μL of a bacterial suspension (1×10^7 CFU/mL) was added to 19.8 mL of prewarmed CAMHB in sterile 50 mL polypropylene tubes resulting in an initial inoculum of 1×10^5 CFU/mL. Antibiotic nanoformulations were added into 20 mL of inoculated CAMHB, desired concentrations were adjusted according to MIC of the ATCC (27853) and clinical (23) strains of *P. aeruginosa*, and tubes were incubated in a shaker at 37 °C. The growth controls in sterile antibiotic-free CAMHB were treated similarly. For total viable counting, serial samples were collected aseptically at different time intervals of 0, 2, 4, 6, 8, 12, and 24 h. Centrifugation of samples was performed for 5 min at 15000 rpm and resuspended in PBS. Further, 100 μL of appropriately diluted sample was then plated on CAMH agar plates manually for total viable counting. And plates were incubated at 37 °C for 24 h and the colonies were counted.[60]

2.13. Statistical Analysis. All experiments were performed in triplicate except where otherwise stated. One-way ANOVA and posthoc Tukey's tests were applied to analyze the data where applicable.

3. RESULTS AND DISCUSSION

3.1. Characterization of the Functionalized Nanosystems. The morphology of MER loaded MCM-41 and its functionalized MSNs was characterized using TEM. These spherical MSNs with slightly rough outer surfaces showed a

https://dx.doi.org/10.1021/acsbiomaterials.0c01284
ACS Biomater. Sci. Eng. 2021, 7, 1836−1853

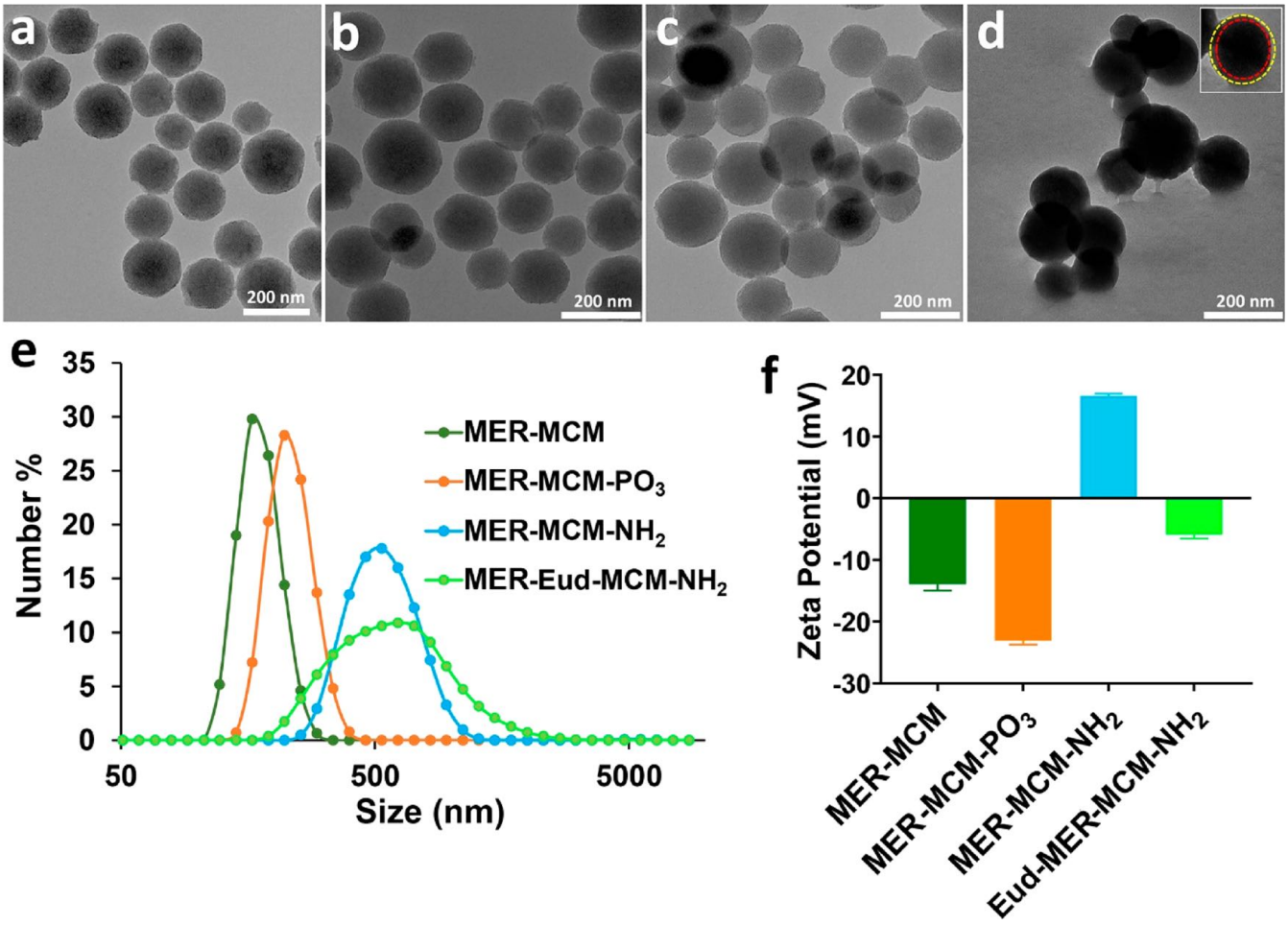

Figure 1. Transmission electron microscope (TEM) images and dynamic light scattering (DLS) data. TEM images of MER loaded particles: (a) MER-MCM, (b) MER-MCM-PO_3, (c) MER-MCM-NH_2, (d) MER-Eud-MCM-NH_2. In the inset, the red dotted circle marks the MSN particle, and the yellow dashed circle labels the Eud S100 coated MSN. All the particles retained their porous morphology after MER loading, and a coating can be seen in the TEM image of MER-MCM-NH_2, confirming the successful electrostatic coating of Eud S100. (e) DLS hydrodynamic diameter of particles analyzed by suspending in water. (f) Zeta potential of the particles measured using DLS.

highly ordered mesoporous network with hexagonal pores (Figure 1). The chemical modification of MCM-41 did not induce any morphological change in the shape or structure of both functionalized particles (MCM-NH_2 and MCM-PO_3) (Figure S1a−c, Supporting Information). The average diameter of MER loaded particles (Figure 1a−c) was around 141 nm, which was quite similar to the average size of unloaded particles (Figure S1a−c, Supporting Information). The bridging phenomenon and thin layer of coating clearly evident in Eudragit S-100 coated MER-MCM-NH_2 (Eud-MER-MCM-NH_2) (Figure 1d, Figure S1d, Supporting Information) suggest that polymer is successfully coated onto silica particles. After the polymer coating, the average size of coated particles was only increased slightly to approximately 150 nm when measured via TEM (Figure 1d, S1d).

Dynamic light scattering (DLS) data including number mean and zeta potential is shown in Figure 1e, f and Table S1 (Supporting Information). As Figure S1 (Supporting Information) shows, the zeta potentials of MCM-41 and MCM-PO_3 were −16 mV and −28 mV, respectively, while the zeta potential of MCM-NH_2 was +15 mV, confirming successful -PO_3 and -NH_2 functionalization. In the case of Eud-MCM-NH_2, the zeta potential was shifted to −11 mV, showing successful coating of negatively charged Eudragit S100. The average size (141 nm) of MCM-41 from TEM was approximately similar to their hydrodynamic size (140 nm) from DLS. However, the hydrodynamic size of MCM-PO_3 and MCM-NH_2 was significantly increased to 206 and 254 nm, respectively, when dispersed in water. Furthermore, hydrodynamic diameters of Eud-MCM-NH_2 (549 nm) and Eud-MER-MCM-NH_2 (645 nm) were almost double than uncoated (MCM-NH_2, 254 nm) and uncoated drug loaded (MER-MCM-NH_2, 288 nm) particles Table S1 (Supporting Information). This increase in hydrodynamic diameter is attributed to the low negative zeta potential of Eud-MCM-NH_2 (−11 mV) and Eud-MER-MCM-NH_2 (−9 mV) that may lead to the agglomeration and is evident in the TEM (Figure 1d) in the form of polymer bridging.

Field emission scanning electron microscopy (FE-SEM) was used to investigate the morphology of MSNs (Figure S2, Supporting Information). SEM images showed that MCM-41 and its functionalized particles were spherical with a size of approximately 140 nm. All the particles were spherical even after functionalization and drug loading (Figure 2S a-c, Supporting Information), which confirmed our TEM results. Further, EDXS spectra confirmed the presence of SiO_2 (Figure 2S g-I, Supporting Information). The pore size and BET (Brunauer−Emmett−Teller) surface area of MSNs were

https://dx.doi.org/10.1021/acsbiomaterials.0c01284
ACS Biomater. Sci. Eng. 2021, 7, 1836−1853

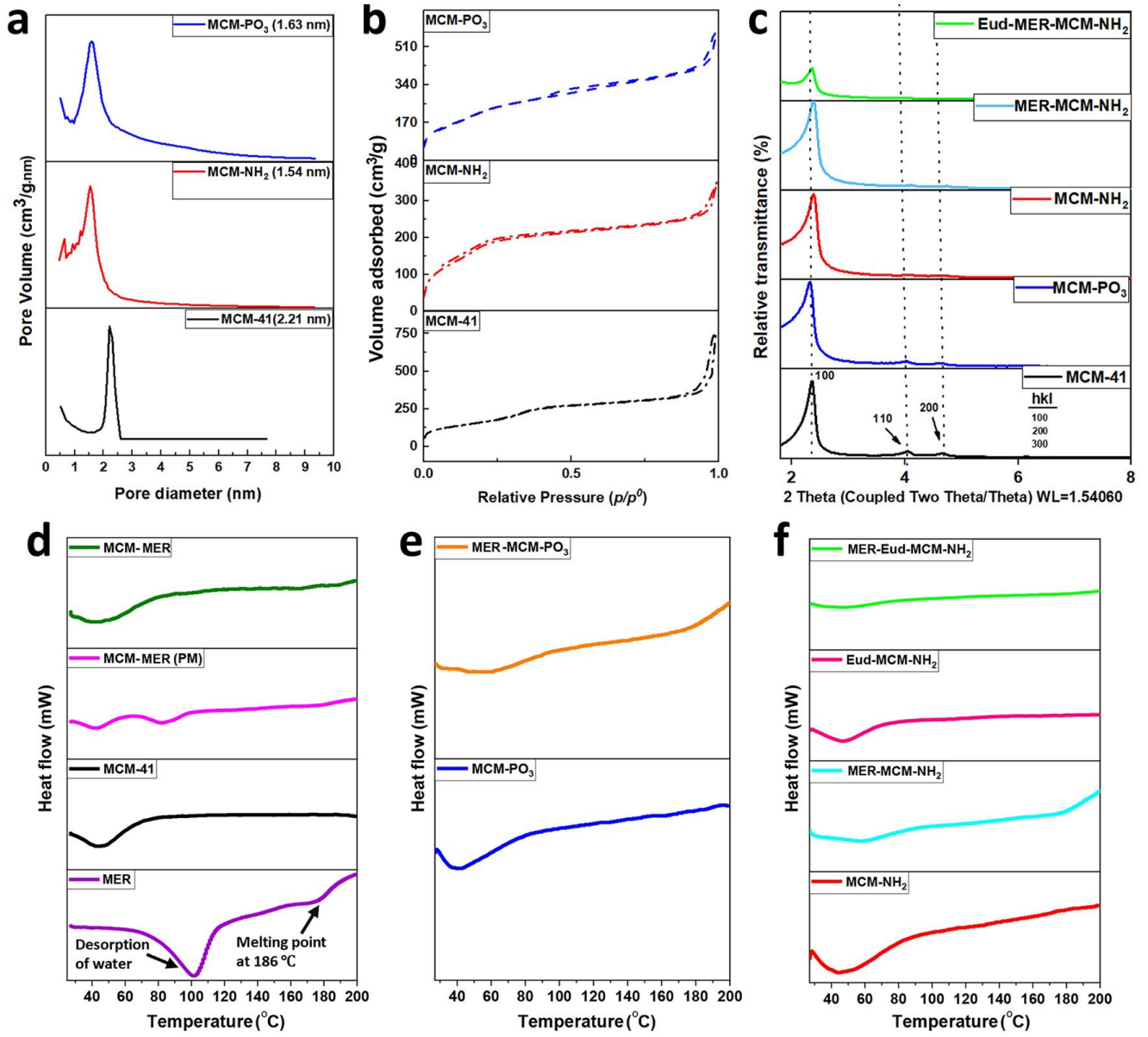

Figure 2. (a) BJH pore size distribution of pristine and functionalized particles (MCM-NH_2 and MCM-PO_3). (b) N_2-BET plot for pristine and chemically functionalized particles. The particles exhibit an IUPAC-type IV isotherm and retain the porous architecture after chemical modifications. (c) Small-angle XRD peaks of MCM-41, MCM-PO_3, MCM-NH_2, MER-MCM-NH_2, and Eud-MER-MCM-NH_2. (d–f) DSC of unloaded and drug-loaded pristine, functionalized, and polymer-coated particles.

measured by nitrogen (N_2) adsorption–desorption isotherm analysis (Figure 2a, b). IUPAC type IV isotherm was displayed by pristine and functionalized MSNs in N_2 sorption analysis, revealing the characteristics of the mesoporous nature of silica nanoparticles. As shown in Table 1S (Supporting Information), the BET surface area of MCM-41 was 941.35 m^2/g, which was decreased after functionalization for MCM-NH_2 (636.33 m^2/g) and MCM-PO_3 (827.15 m^2/g). It was important to note that the BET surface areas of MER loaded MCM-41, MCM-NH_2, and MCM-PO_3 were further reduced to 343.26, 115.89, and 149.42 m^2/g, respectively. The BJH pore size of MCM-41 (2.21 nm) was also decreased upon -PO_3 (1.58 nm) and -NH_2 (1.54 nm) surface functionalization. Similarly, the pore volume of MCM-41 (0.93 cm^3/g) decreased considerably for MCM-NH_2(0.51 cm^3/g), while it changed for MCM-PO_3(0.81 cm^3/g). All these changes in the physical properties of MSNs upon surface modification were similar to our previously reported results.[34,37,61]

Small-angle X-ray scattering (SAXS) analysis was performed to further confirm the ordered mesoporous structure of MSNs (Figure 2c). Three well-resolved peaks with hkl values of 100, 110, and 200, respectively, confirmed two-dimensional (2D) hexagonal mesopores of MSNs (Figure 2c). There was a slight right shift in diffraction peaks of MCM-NH_2 and MCM-PO_3, which suggest a small change in pore size due to functionalization but not in their symmetry.[37] After MER loading, the intensity of the peaks decreased, confirming the filling of the pores. Further, Eud-MER-MCM-NH_2 showed only one diffraction peak (100) with weaker intensity, confirming the presence of an additional polymeric layer of Eudragit S100 (Figure 2c).

The DSC thermogram of pure MER (Figure 2d) showed a sharp endothermic peak for water desorption at 110 °C and an

https://dx.doi.org/10.1021/acsbiomaterials.0c01284
ACS Biomater. Sci. Eng. 2021, 7, 1836–1853

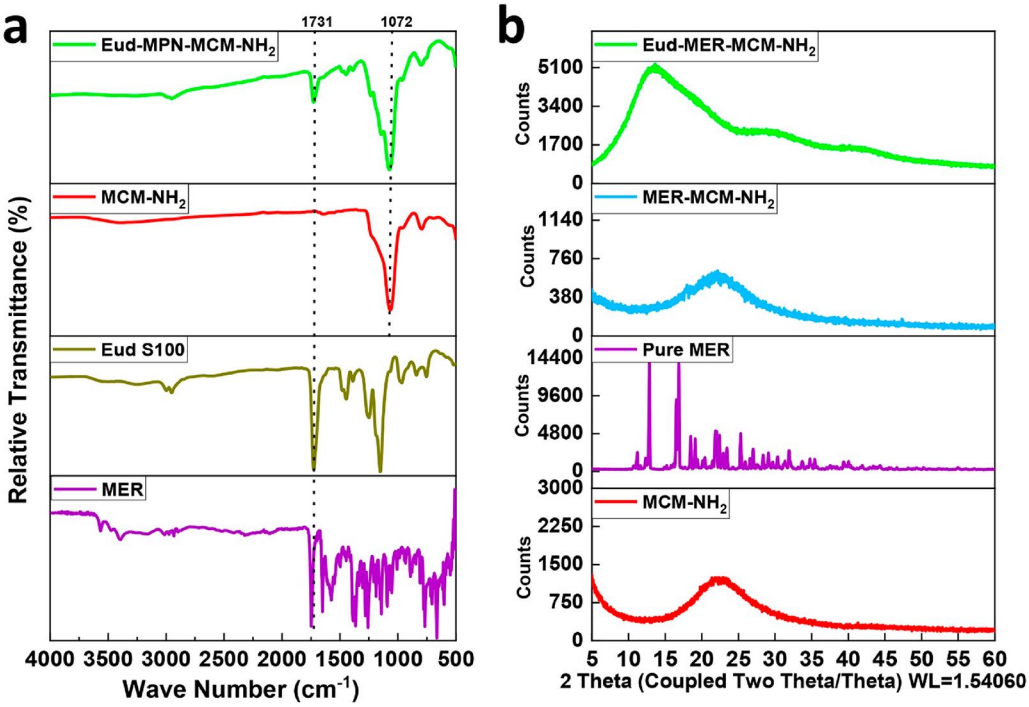

Figure 3. (a) Fourier transform infrared (FTIR) spectroscopy of MER, Eud S 100, MCM-NH2, and Eud-MER-MCM-NH_2 particles for range 500 cm^{-1} to 4000 cm^{-1}. (b) Wide-angle X-ray diffractograms (WXRD) of MCM-NH_2, MER MCM-NH_2, and Eud-MER-MCM-NH_2 particles where only the MER shows crystalline peaks while no crystalline peaks are observed for any other formulation.

endothermic peak, representing the melting point at 186 °C. This analysis confirmed the crystalline nature of MER. However, both water desorption and melting point peaks were not observed in the DSC thermograms of MER loaded MSNs, confirming successful loading of drug into pores of MSNs. Whereas the physical mixture (PM) of MER and MCM-41 showed both endothermic peaks in the DSC thermogram, the absence of such peaks in the case of all the drug-loaded particles proves the successful loading of MER into particles and its amorphous state (Figure 2d–f).

Drug loading and surface functionalization of MSNs were also analyzed using Fourier transform infrared (FTIR) spectroscopy. As shown in Figure 3, MER displayed broad peaks at 3568 and 3401 cm^{-1} that are attributed to -OH and -NH stretching, respectively. A sharp peak at 1750 cm^{-1} corresponds to C═O stretching in COOH and pyrrolidine ring. Other peaks at 1188 and 668 cm^{-1} are ascribed to -CN stretching in pyrrolidine ring and -OH bending in COOH, respectively. In the case of MCM-41, a band at 3437 cm^{-1} is related to the stretching vibration of -OH groups (Si–OH), while other characteristic peaks at 1072 and 805 cm^{-1} are assigned to Si–O and Si–O–Si vibrations of silanol groups. Similar peaks were also observed after the salinization (PO_3 and NH_2) of MCM-41. Also, some characteristic peaks at 1640 and 1525 cm^{-1} were attributed to NH_2 bending and aminopropyl groups, respectively,[62,63] confirming the successful functionalization of amino groups onto MCM-41 (Figure S3a, Supporting Information). Furthermore, IR absorption bands of phosphonate groups were not observed from 800 to 1200 cm^{-1} due to the overlapping of Si–O–Si vibrations in this region (Figure S3a, Supporting Information).[64] A broad band at 3442 cm^{-1} (OH bonding) and a sharp peak at 1731 cm^{-1} (C═O stretching) were observed in the FTIR spectrum of Eudragit S100.[64,65] It is noteworthy that a characteristic peak of MER at 1750 cm^{-1} with weaker intensity could be seen in all drug-loaded MSNs except Eud-MER-MCM-NH_2, where a characteristic band of Eudragit S100 at 1731 cm^{-1} is more clear and overlapping the MER band. It affirms the coating of Eudragit S100 around MER-MCM-NH_2 (Figure 3a).

It is well-known that the loading of drugs into mesopores not only changes the structure of drugs from crystalline to amorphous but also prevents them from recrystallization.[61] To confirm this, wide-angle XRD was performed for both MER loaded and unloaded MSNs as well as their coated particles. MER was observed with multiple XRD peaks at 2θ of 12.74, 16.85, and 25.49, etc. due to its crystalline nature (Figure 3b). However, crystalline peaks of MER were not observed in any drug-loaded MSNs with or without coating, confirming the amorphization of the drug inside the pores of MSNs[34,61,66] (Figure 3b, S4a and b, Supporting Information). However, the physical mixture of MER and MCM-41 displayed the characteristic crystalline peaks of pure MER, confirming the need for the encapsulation or adsorption process (Figure S4a, Supporting Information).

TGA was performed to determine the % mass grafting of functional groups (PO_3 and NH_2) after surface functionalization of MCM-41. The thermograms (Figure S5a Supporting Information) show that % mass grafting with APTES (MCM-NH_2, 12.8%) was considerably higher than THMP (MCM-PO_3, 3.3%).

3.2. MER Loading and Cy-5 Grafting. MER (around 30% *w/w*) was loaded into MCM-41 using liquid CO_2. TGA was used to determine the loading capacity of MER by calculating weight loss. Figure S5 b (Supporting Information) shows a 27.5 *wt* % of MER loading onto MCM-41 using the liquid CO_2 in 4 h. As a control, MER was also loaded onto MCM-41 using a more traditional immersion loading method, which resulted in a 25.3 *wt* % MER loading. With these

https://dx.doi.org/10.1021/acsbiomaterials.0c01284
ACS Biomater. Sci. Eng. 2021, 7, 1836–1853

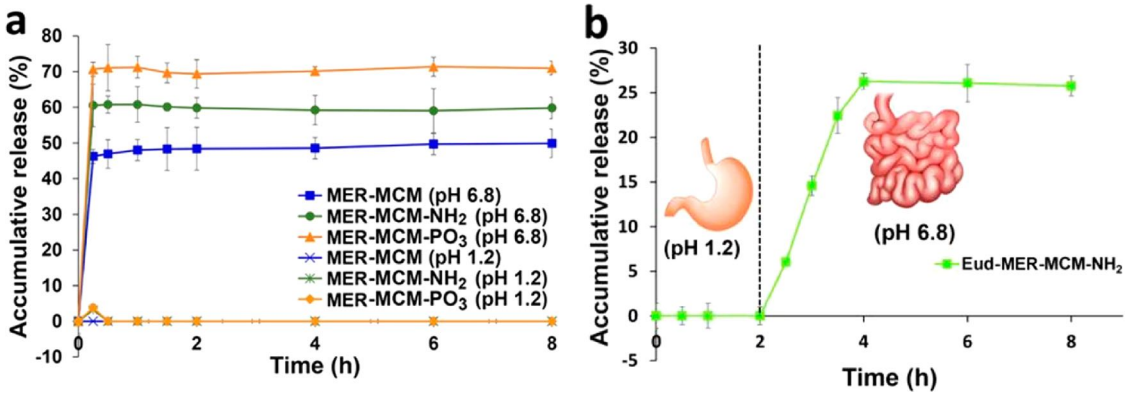

Figure 4. (a) MER release profile from MCM and functionalized MCM particles was conducted in 5 mL of simulated gastric (pH 1.2) and intestinal (pH 6.8) media at 37 °C. The MCM-41, MCM-PO_3, and MCM-NH_2 particles suppress the release of MER up to 46%, 60%, and 70%, respectively, at pH 6.8 in 8 h. However, MER was degraded at gastric pH and no stable drug was detected after 30 min. (b) MER release profile from Eud-MER-MCM-NH_2 particles in the universal buffer (gastric pH for 2h, intestinal pH for 6 h) at 37 °C. In the first 2 h, no MER is released showing that polymer could protect the drug from degradation in gastric fluid. However, coated particles suppress MER release up to 25.7% at pH 6.8 in 6 h (n = 3 ± SD).

encouraging drug loading results, the liquid CO_2 method was selected for further drug loading experiments based on its high drug loading in a shorter (4 h) duration without the need of a further freeze-drying step.

TGA thermograms (Figure S5c, d Supporting Information) illustrated that 25.4% and 31.2% of MER was loaded into MCM-NH_2 and MCM-PO_3 using liquid CO_2. It was worth noting that loading capacity in all our formulation was between 25 and 31% *w/w*, confirming excellent loading capacity achieved with our novel loading method in comparison to the literature.[29,30] For MSNs coating, we selected negatively charged Eudragit S100 for coating on positively charged MER-MCM-NH_2. To minimize the leaching of MER from preloaded nanoparticles, a simple immersion method was used for the coating process rather than liquid CO_2. We used ethanol as a solvent in a coating process where Eudragit S100 was soluble but MER was insoluble. TGA data (Figure S 5f, Supporting Information) showed that the loading capacity of MER was 24.1 *wt* % in Eud-MER-MCM-NH_2 with minimal drug leaching of 1.3 *wt* %. DSC analysis was also performed in parallel to TGA to confirm that weight loss for drug loading is observed from the drug-loaded into the pores of MSNs rather than drug adsorbed on the outer surface of MSNs.

To investigate the quantitative (flow cytometry) and qualitative (confocal microscopy) intracellular uptake of MSNs, it was necessary to develop fluorescent MSNs. It has been reported that cyanine dyes have been covalently conjugated with APTES to successfully achieve their loading into silica particles.[67,68] Therefore, Eudragit S100 coated Cy5-MCM-NH_2 (Eud-Cy5-MCM) was selected for fluorescence imaging and flow cytometry studies.

The immersion method was used to covalently attach the Cy-5 dye onto MCM-NH_2. TGA analysis was performed to determine the dye loading capacity. The TGA thermogram (Figure S5g, Supporting Information) showed that 9% (*w/w*) of Cy-5 dye was attached to MCM-NH_2.

3.3. *In Vitro* Release Study of MER. MER's poor oral bioavailability is mainly due to the degradation in acidic gastric pH and poor permeability due to drug efflux, which we have tackled by our innovative formulation approach. The digestive enzymes do not have any impact on stability or applicability of MER.[20,22] To further potentiate our claim, we verified that there was no considerable difference in MER degradation (no stable drug detected) in simulated gastric fluid (SGF) with and without digestive enzymes (Figure S6a, b, Supporting Information) after 8 h of incubation. In the case of SGF both types of media degraded almost all of the added MER. While in simulated intestinal fluid (SIF), 87% and 96% of active MER were detected with and without digestive enzymes (Figure S6c, d, Supporting Information), respectively. Therefore, simulated gastric and intestinal fluids without digestive enzymes were used in our *in vitro* drug release studies.

As shown in Figure 4a and S7b,c (Supporting Information), suspending uncoated MSNs in simulated gastric solution (pH 1.2) resulted in 3.24% and 3.77% of MER release (stable form) from MCM-NH_2 and MCM-PO_3, respectively, in the first 15 min. After that, MER was degraded at gastric pH and no stable drug was detected. At intestinal pH (pH 6.8), burst release of drug at 46%, 60%, and 70% could be seen from MCM-41, MCM-NH_2, and MCM-PO_3, respectively, after 15 min. Moreover, it was interesting to note that there was no significant improvement in drug release from all MSNs after the initial burst in which MCM-PO_3 displayed the highest release. A similar pattern of drug release profile from MSNs was reported for a hydrophilic drug (Doxorubicin), where only about 60% of the total drug was released after 70 h.[69] The study showed that this drug has more hydrogen acceptor (12) counts as compared to hydrogen donor counts (6). Therefore, the drug was strongly bonded with MCM-41 due to hydrogen bonding, which resulted in incomplete drug release even after 70 h. Similarly, the Meropenem trihydrate (MER·$3H_2O$) that was used in this study is also identified with a 10-hydrogen acceptor and six hydrogen donor counts.[70] We believe that hydrogen bonding between MER and MSNs could be one of the reasons for incomplete drug release after 8 h which needs to be further investigated.

Later, we used a universal buffer to evaluate the drug release profile from Eudragit S-100 coated MSNs. As seen from Figure 4b and S7d (Supporting Information), there was no MER release from Eud-MER-MCM-NH_2 within 2 h at simulated gastric pH (pH 1.2). It showed that polymer could protect the drug from degradation in gastric fluid. At the simulated intestinal pH condition (pH 6.8), the controlled release of drug from coated particles was observed and around 25.7% of

https://dx.doi.org/10.1021/acsbiomaterials.0c01284
ACS Biomater. Sci. Eng. 2021, 7, 1836−1853

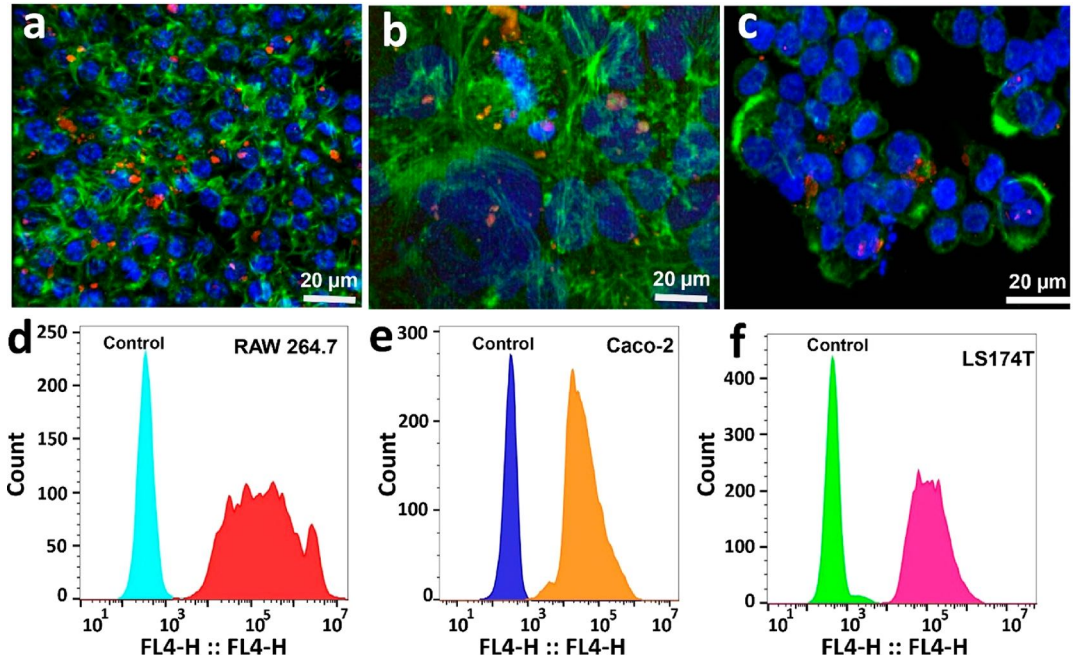

Figure 5. Confocal images (a–c) of the uptake of Eud-Cy5-MCM (100 μg/mL) following 2 h incubation with (a) RAW 264.7 macrophages, (b) Caco-2 cells, and (c) LS174T. The filamentous actin cytoskeleton of cells was stained with Phalloidin-FITC and is shown in green. The cell nuclei were stained with DAPI and are shown in blue. Cy5 loaded particles fluoresce red. Sections through the cells showed that the Cy5 signal was located intracellularly rather than being adsorbed onto the cell surface. Flow cytometry histograms (d–f) showing the uptake of Eud-Cy5-MCM (100 μg/mL) following 2 h incubation at 37 °C with (d) RAW 264.7, (e) Caco-2 cells, and (f) LS174T, respectively. The fluorescence intensity of all three cell types was increased as compared to their controls after their treatment with Eud-Cy5-MCM, confirming the cellular uptake of dye loaded nanoparticles.

the drug was released in 6 h. The drug release from coated particles was related to the ionization of carboxyl groups of the polymer upon a sudden increase in pH from 1.2 to 6.8.[71] Conclusively, this study revealed the pH-sensitive release of MER at simulated intestinal pH as well as its protection from degradation at stimulated gastric pH (Figure S7, Supporting Information).

3.4. *In Vitro* Cytocompatibility of MCM-NH_2 and Eud-MCM-NH_2. In this assay, three cell lines including Raw 264.7 macrophages and two intestinal epithelial adenocarcinoma cell lines (enterocyte-like Caco-2 and goblet cell-like LS174T) were used to evaluate the *in vitro* cytocompatibility of MCM-NH_2 and Eud-MCM-NH_2. To investigate the influence of the coating on amine-functionalized silica particles, these cells were treated with six different concentrations (25 μg/mL to 1000 ug/mL) of particles for an incubation time of 24 h. As seen from Figure S8 (Supporting Information), no significant difference in cytoviability for both of these particles was observed in all three cell lines up to the concentration of 100 μg/mL. However, at higher concentrations (250–1000 μg/mL), Eud-MCM-NH_2 was found to be less cytotoxic as compared to uncoated MCM-NH_2 in both the intestinal cancer cell lines. Overall, the highest tested concentrations of coated silica particles were relatively nontoxic, which is in agreement with previous studies.[66,72]

3.5. Cell Uptake and Intracellular Distribution of Nanoparticles. *3.5.1. Qualitative Intracellular Uptake Measure by Confocal Microscopy.* Trans- and paracellular are the two most common pathways for the drugs to permeate through the intestinal epithelium. Cellular internalization of the drugs via nanoparticles is a promising strategy to provide valuable information about the transcellular uptake of drugs. To investigate this phenomenon, the Eudragit coated Cy-5 grafted silica particles (MCM-NH_2) were used. Briefly, Eud-Cy5-MCM particles were incubated for 4 h with different cells including RAW 264.7 macrophages and intestinal cancer cells (Caco-2 and LS174T). After cell fixation, fluorescent reagent such as DAPI (blue color) and phalloidin-FITC (green color) was used to visualize the nucleus and cytoskeleton of the cells, respectively. To confirm whether Eud-Cy5-MCM is internalized or simply adsorbed onto the surface of cells, images for all cell types were taken at multiple confocal depths (z-sections) using confocal microscopy. As depicted in Figure 5a–c, red fluorescent Eud-Cy5-MCM nanoparticles were observed to be distributed throughout the cytoplasm of all cell types tested here, indicating that our nanoparticles could have the potential to carry any drug to internalize into the cells.

3.5.2. Quantitative Cellular Uptake Measured by Flow Cytometry. To confirm the results of confocal microscopy quantitatively, all three cell types were incubated (2 h) with Eud-Cy5-MCM to calculate the cellular uptake of nanoparticles using flow cytometry. As shown in the histograms (Figure 5d–f), the fluorescence intensity of all three cell types was increased as compared to their controls after their treatment with Eud-Cy5-MCM, confirming the cellular uptake of dye loaded nanoparticles. Importantly, Raw 264.7 macrophages were identified with high cellular uptake (over 400000 arbitrary units, 89.7%) based on their median fluorescence intensity followed by LS174T (over 250000 arbitrary unit, 86.8%) and Caco-2 cells (over 60000 arbitrary unit, 73.9%) (Figure S9). Overall, this data indicated that Eud-Cy5-MCM was internalized in all three cell lines within 2 h.

3.5.3. TEM and STEM-EDXS Based Visual and Molecular Cellular Uptake. We further evaluated the cellular uptake of

https://dx.doi.org/10.1021/acsbiomaterials.0c01284
ACS Biomater. Sci. Eng. 2021, 7, 1836–1853

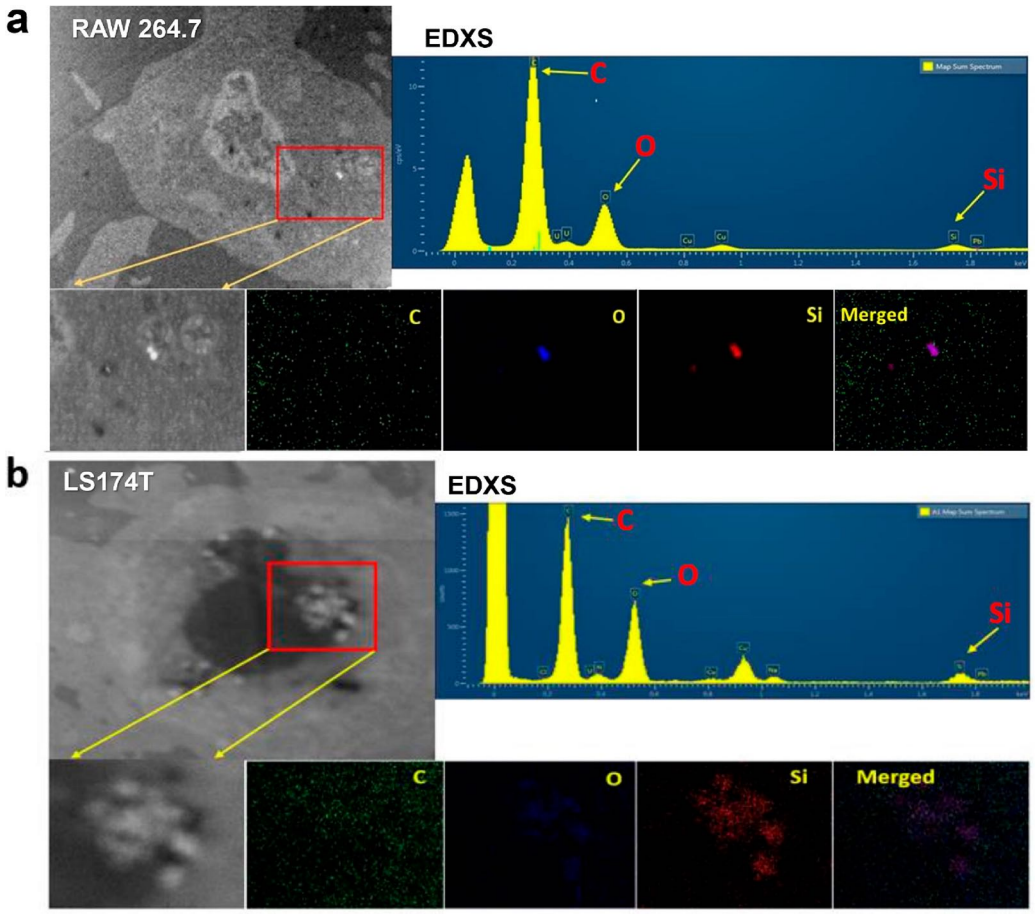

Figure 6. STEM mapping of Eud-MCM-NH_2 nanoparticles inside (a) RAW 264.7 macrophage (30 min incubation) and (b) LS174T (3 h incubation). The location of nanoparticles, detected by STEM, appeared as bright white dots as shown in the red box. Elemental mapping of C, shown in green; O, shown in blue; and Si, shown in red. Merged images of O, C, and Si (shown in purple) confirmed the identity of the silica drug delivery system in the cell. EDXS spectrum showing each elemental peak of intracellular Eud-MCM-NH_2 nanoparticles.

coated nanoparticles (Eud-MCM-NH_2) using TEM and STEM-EDXS (Figure 6). Raw 264.7 macrophages and LS174T were selected for further investigation of drug-loaded particles. Thin sections of cells obtained by ultramicrotome were mounted onto TEM grids and examined to investigate the location of particles. Interestingly, different cell organelles such as the nucleus, mitochondria, and vacuole were also clearly identified. As shown in Figure S10 (Supporting Information), black dots were visually identified as particles in bright field TEM that could be seen inside and outside the cells. After 30 min of incubation of nanoparticles (50 μg/mL), nanoparticles were observed in macrophages but particles were not detected inside LS174T. Therefore, LS174T cells were further incubated with Eud-MCM-NH_2 (100 μg/mL) for 3 h, resulting in the penetration of particles (Figure S11, Supporting Information). To confirm that these black dots were not artifact or resin embedded cellular debris, these thin sections were further examined under dark field STEM-EDXS. It is worth noting that these black dots were identified as white dots in the dark field and their elemental composition was determined using EDXS (Figure 5). Elemental mapping results showed that these white dots are composed of carbon (C), oxygen (O), and silicon (Si), confirming them as silica particles as well as their cellular internalization. Conclusively, Eud-MCM-NH_2 nanoparticles have the potential to provide intracellular drug delivery.

3.6. *In Vitro* Permeability Assay. To predict the permeability profile of MER and its nanoparticles, the Caco-2 monolayer culture model was used because it is known for both absorptive (A to B) and secretory (B to A) characteristics of epithelial intestinal cells. Therefore, the bidirectional transport of MER and its nanoparticles (MER equivalent concentration of 200 μg/mL) was performed across the Caco-2 monolayer at different time points (1 and 2 h). As shown in Figure 7, MER-MCM-NH_2 and Eud-MER-MCM-NH_2 were observed to significantly enhance the absorptive transport of MER as compared to MER solution at different time points of 1 and 2 h. This improved permeation of MER using MER-MCM-NH_2 and Eud-MER-MCM-NH_2 was around 1.9-fold and 2.4-fold, respectively. For drug secretory transport, it was worth noting that Eud-MER-MCM-NH_2 was able to significantly reduce (~1.8-fold) the MER secretion across the Caco-2 monolayer, confirming the potential of Eudragit S-100 and silica particles to reduce drug efflux. According to Figure 7c, the apparent permeability coefficient (P_{app}) (A to B) values are 0.96 × 10^{-6} cm/s, 1.46 × 10^{-6} cm/s, and 1.82 × 10^{-6} cm/s for MER, MER-MCM-NH_2, and Eud-MER-MCM-NH_2, respectively. For secretory transport, the Papp (B to A) values were 2.63 × 10^{-6} cm/s, 1.68 × 10^{-6} cm/s, and 1.19 × 10^{-6} cm/s for MER, MER-MCM-NH_2, and Eud-MER-MCM-NH_2, respectively. It is reported in different studies that drugs with P_{app} > 10^{-6} cm/s presented excellent oral bioavail-

https://dx.doi.org/10.1021/acsbiomaterials.0c01284
ACS Biomater. Sci. Eng. 2021, 7, 1836−1853

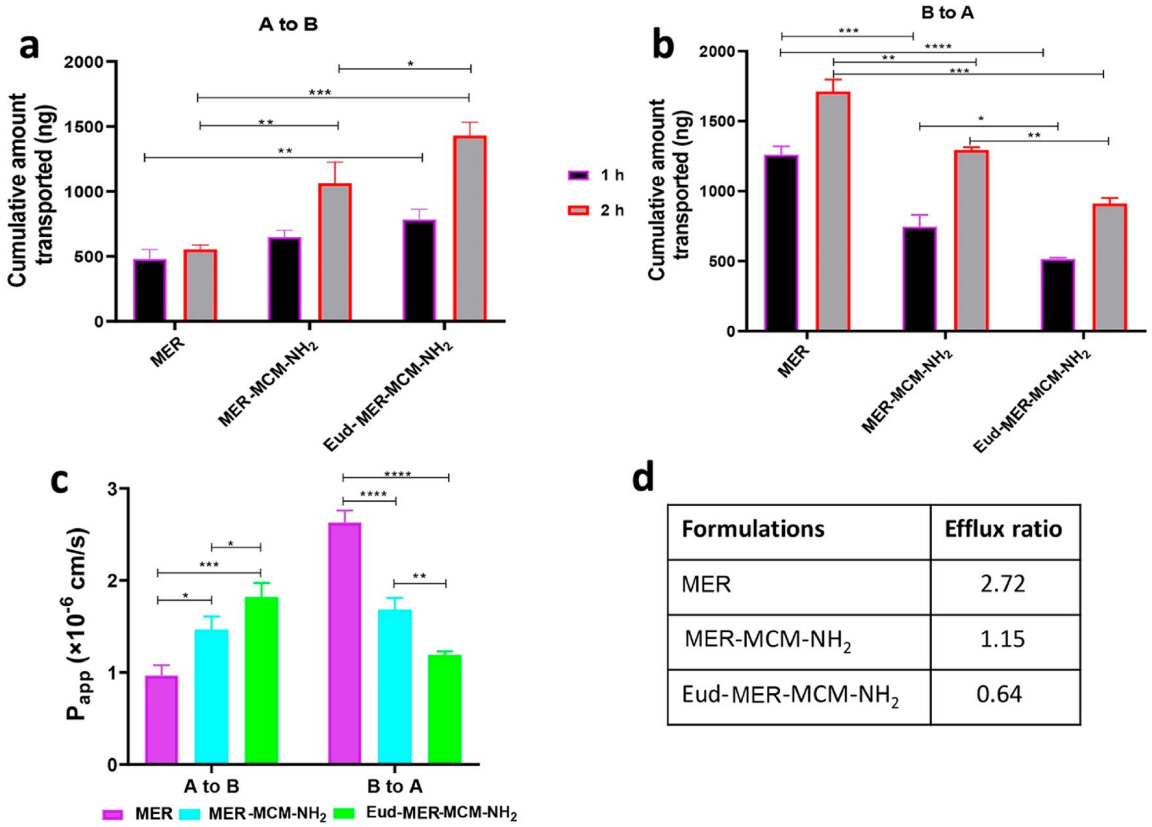

Figure 7. Cumulative amount of MER transported (a) A to B and (b) B to A through the Caco-2 monolayer at 1 and 2 h, where monolayers were incubated with MPM, MER-MCM-NH_2, and Eud- MER-MCM-NH_2 solutions (MER equivalent concentration of 200 μg/mL) (all data are $n = 3$, mean ± SD, and analyzed by one-way ANOVA, posthoc Tukey's test, * $p < 0.01$, ** $p < 0.0036$, *** $p < 0.0002$, **** $p < 0.0001$). (c) Apparent permeability coefficient (P_{app}) of MER from MER-MCM-NH_2 and Eud- MER-MCM-NH_2 at 2 h in the Caco-2 monolayer (all data are $n = 3$, mean ± SD, and analyzed by one-way ANOVA, posthoc Tukey's test, * $p < 0.05$, ** $p < 0.0036$, *** $p < 0.0006$, **** $p < 0.0001$). (d) Efflux ratio for MER, MER-MCM-NH_2, and Eud- MER-MCM-NH_2.

ability;[73,74] therefore, Eud-MER-MCM-NH_2 could be a suitable candidate for further oral drug absorption evaluation. In addition, the efflux ratio (ER) values (Figure 7d) were 2.72, 1.15, and 0.65 for MER, MER-MCM-NH_2, and Eud-MER-MCM-NH_2, respectively, indicating a marked decrease in the efflux of MER using uncoated and coated functionalized nanoparticles. However, other studies with complex *in vitro* and *in vivo* models are still required to investigate the exact mechanism of drug transport (absorptive and secretory) across the Caco-2 monolayer.[75]

Next, a recovery experiment based on TEER values was performed to evaluate the integrity of the Caco-2 monolayer after treatment with our formulations. After 2 h of permeability experiment, the monolayer was washed thrice with DMEM media to remove any particle on the Caco-2 monolayer. TEER values were noted at different time points (0, 2, 4, 8, and 24 h). Figure S12 (Supporting Information) illustrates that the integrity of the Caco-2 monolayer was recovered within 24 h, confirming TEER decrease at the 2 h time point was transient and our formulations were nontoxic.

The increase in permeability of MER could be due to the following reasons: including (i) transient opening of tight junctions by silica nanoparticles or drug-loaded silica nanoparticles and (ii) permeation of drug across the cell monolayer via cellular endocytosis and exocytosis of nanoparticles.[76] Also, many studies have shown that the energy-dependent endocytosis of MSNs could inhibit or downregulate the P-gp efflux pump, resulting in a bypass from efflux.[77−80] Furthermore, it is well reported that polymethacrylate polymers (Eudragit S100, RS100, L50-100, etc.) have the ability to downregulate the P-gp efflux pump[50,81−83] or could help the drug to escape from P-gp because the pump does not recognize drug due to polymer coating.[82,84] Therefore, the improvement in permeation and decrease in secretory transport of MER across the Caco-2 monolayer could be attributed to the following reasons: (1) The efficient cellular uptake of Eudragit coated particles which is evident from confocal microscopy, flow cytometry, and STEM-EDXS demonstrated that MER could be efficiently delivered into Caco-2 cells and may help in transcellular drug transport. (2) The pH-responsive release of MER could reduce the drug degradation outside the cells and increase the intracellular drug concentration. (3) The sustained intracellular release ability of MER could reduce drug efflux by P-gp because the free MER was the substrate of P-gp rather than the nanoparticles. (4) The inhibitory or downregulatory effects of Eudragit on the P-gp efflux pump could further suppress drug efflux, which might be responsible for enhanced paracellular drug transport. Nevertheless, other studies with complex *in vitro* and *in vivo* models are still required to investigate the exact mechanism of Eudragit to suppress the P-gp efflux pump in Caco-2 cells.[50,77,82,85]

3.7. *In Vitro* Antibacterial Activity of MER-Loaded Nanoparticles. The minimum inhibitory concentration (MIC_{90}) of MER-loaded nanoparticles was investigated using broth microdilution followed by EUCAST guidelines. We used

https://dx.doi.org/10.1021/acsbiomaterials.0c01284
ACS Biomater. Sci. Eng. 2021, 7, 1836−1853

both Gram-positive (*S. aureus*) and Gram-negative (*P. aeruginosa*) species of bacteria to determine the antibacterial effect of MER formulations. According to EUCAST guidelines, the MIC ranges of MER against ATCC strains of *P. aeruginosa* and *S. aureus* are 0.125−1 mg/L[86] and 0.03−0.12 mg/mL,[87] respectively. As summarized in Table 1, MIC values for MER

Table 1. Values of MIC (mg/L) of MER and MER Loaded Particles against ATCC and Clinical Isolates of Selected Gram-Negative (*P. aeruginosa*) and Gram-Positive Bacteria (*S. aureus*)

	P. aeruginosa (mg/L)		*S. aureus* (mg/L)	
Formulations	ATCC	clinical strain 23	ATCC	clinical strain 54
MER	1	0.5	0.125	0.0625
MER-MCM-41	0.5	0.25	0.0625	0.0625
MER-MCM-NH_2	0.5	0.25	0.125	0.0625
MER-MCM-PO_3	0.5	0.25	0.0625	0.0625
MER-MCM-NH_2−Eud	0.5	0.5	0.125	0.125

free drug against reference and clinical strains of *P. aeruginosa* are 1 and 0.5 mg/L, respectively. However, all of our MER nanoformulations showed half of the MIC against ATCC and clinical strains of *P. aeruginosa* as compared to free MER, which is 0.5 and 0.25 mg/L, respectively. For ATCC and clinical strains of *S. aureus*, the MIC values of free MER are 0.125 and 0.0625 mg/L, respectively. In the case of nanoformulations, the MIC values of MER-MCM-NH_2 and Eud-MER-MCM-NH_2 are similar to free drug against the ATCC strain of *S. aureus*. However, half of the MIC values of MER-MCM and MER-MCM-PO_3 as compared to MER were noticed against the ATCC strain of *S. aureus*. Interestingly, MIC values of all nanoformulation against the clinical strain of *S. aureus* were similar to MER except Eud-MER-MCM-41 (0.125 mg/L). The above results show that our nanoparticles showed the potential to significantly decrease the MIC values of the pure MER. However, drug-free nanoparticles did not show any antibacterial activity (data not shown here). It has been reported that adsorbed antibiotics on nanoparticles are more effective than antibiotics in solution because antibiotic-loaded nanoparticles could act on the bacteria with high local antibiotic concentration, which led to perforation of the bacterial cell membrane.[88,89] However, based on EUCAST guidelines, the MIC values against all bacterial strains were within the range of free drug, concluding that our nanoparticles were able to retain the antibacterial activity.

3.8. Time-Kill Assay. The time-kill assay was performed to investigate the rate of killing of bacteria by MER and its nanoformulations treatment. Herein, the viability of *P. aeruginosa* (ATCC 27853 and clinical strain 23) was tracked in the presence of free MER and its nanoformulations and compared with controlled untreated culture. As shown in Figure 8a, treating the ATCC strain of *P. aeruginosa* with MER and its formulations resulted in a marked decrease in bacterial growth after 2 h of incubation, and maximal bacterial killing to an undetectable level could be seen within 8 h. Interestingly, the rates of bacterial killing for MER and its nanoformulations were quite similar. However, the count of *P. aeruginosa* (23) significantly reduced from 1×10^5 to 1×10^2 CFU/mL after 2 h of incubation with MER and its nanoformulations and decline to 0 within 4 h, resulting in complete bacterial killing

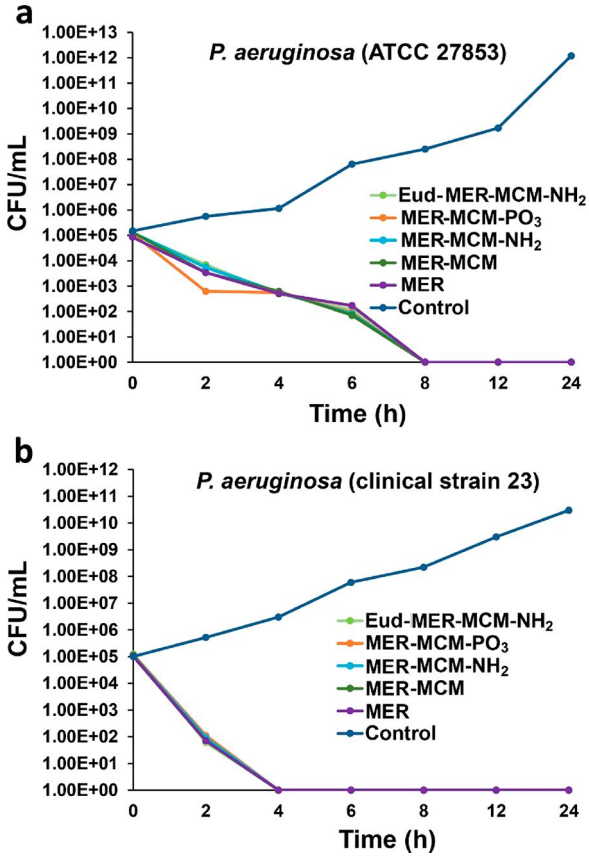

Figure 8. Representative time-kill curves for MER and MER loaded particles against (a) ATCC and (b) clinical isolates of *P. aeruginosa*. As shown in part a, treating the ATCC strain of *P. aeruginosa* with MER and its formulations resulted in a marked decrease in bacterial growth after 2 h of incubation, and maximal bacterial killing to an undetectable level could be seen within 8 h. However, the count of *P. aeruginosa* (23) significantly reduced from 1×10^5 to 1×10^2 CFU/mL after 2 h of incubation with MER and its nanoformulations and declined to 0 within 4 h, resulting in complete bacterial killing (part b).

(Figure 8b). Overall, the rate of killing of MER and its nanoformulations were observed more rapidly against the clinical strain of *P. aeruginosa* as compared to its ATCC strain.

4. CONCLUSION

Designing modern oral formulations and finding new methods to develop efficient antibiotic systems in the current era of antibiotic resistance is extremely important. To the best of our knowledge, this is the very first study to develop oral MER formulations with pH-responsive mesoporous silica nanoparticles. To summarize, MSNs such as MCM-41 were successfully synthesized and functionalized with phosphonate and amine terminals. MCM-PO_3 showed the highest drug loading of 31.2% using liquid CO_2, while positively charged drug-loaded amine-functionalized particles with 25.1% loading were selected for coating with negatively charged Eudragit S-100 to create electrostatic interaction which led to 24.1% final drug loading. *In vitro* release study showed that both pristine and functionalized MSNs showed fast release in basic pH with immediate drug degradation in acidic pH. However, coated cargo loaded particles showed promising potential to protect the drug from gastric degradation with controlled release of drug at simulated intestinal pH. This work also demonstrates

https://dx.doi.org/10.1021/acsbiomaterials.0c01284
ACS Biomater. Sci. Eng. 2021, 7, 1836−1853

the significant potential of particles for intracellular uptake through macrophages and intestinal cancer cells. Our study offers improved permeability of the drug as well as a reduced rate of drug efflux in the Caco-2 cell monolayer model for both drug-loaded uncoated and coated amine-functionalized silica particles. Finally, we show that the encapsulation of Meropenem with pristine, functionalized, and coated silica particles retained MER's antibacterial activities against two bacterial strains. Our proof of concept study paves the way for further comprehensive in vivo studies to explore the exact mechanism of improved drug permeation with reduced drug efflux and the interaction of drug-loaded silica particles with the bacterial cell membrane which could change the way we deliver MER in the clinic.

■ ASSOCIATED CONTENT

Supporting Information

The Supporting Information is available free of charge at https://pubs.acs.org/doi/10.1021/acsbiomaterials.0c01284.

DLS and BET data, TEM and SEM images, FTIR, WXRD, TGA, UHPLC, cell viability study, fluorescence intensity data, bright field TEM images for cells, and TEER recovery (PDF)

■ AUTHOR INFORMATION

Corresponding Authors

James R. Falconer − *School of Pharmacy, The University of Queensland, Woolloongabba, QLD 4102, Australia;* orcid.org/0000-0002-7324-6605; Phone: +61-(7)-3346-1852; Email: j.falconer@uq.edu.au

Tushar Kumeria − *School of Pharmacy, The University of Queensland, Woolloongabba, QLD 4102, Australia; School of Materials Science and Engineering, The University of New South Wales, Sydney, NSW 2052, Australia;* orcid.org/0000-0003-3351-7148; Phone: +61-(2)-9065-4342; Email: t.kumeria@unsw.edu.au

Amirali Popat − *School of Pharmacy, The University of Queensland, Woolloongabba, QLD 4102, Australia; Mater Research Institute, The University of Queensland Translational Research Institute, Woolloongabba, QLD 4102, Australia;* orcid.org/0000-0001-5401-3446; Phone: +61-(7)-3346-1852; Email: a.popat@uq.edu.au

Authors

Aun Raza − *School of Pharmacy and Centre for Translational Anti-infective Pharmacodynamics, School of Pharmacy, The University of Queensland, Woolloongabba, QLD 4102, Australia*

Fekade Bruck Sime − *School of Pharmacy and Centre for Translational Anti-infective Pharmacodynamics, School of Pharmacy, The University of Queensland, Woolloongabba, QLD 4102, Australia*

Peter J. Cabot − *School of Pharmacy, The University of Queensland, Woolloongabba, QLD 4102, Australia*

Jason A. Roberts − *School of Pharmacy and Centre for Translational Anti-infective Pharmacodynamics, School of Pharmacy, The University of Queensland, Woolloongabba, QLD 4102, Australia; Department of Intensive Care Medicine and Department of Pharmacy, Royal Brisbane and Women's Hospital, Brisbane, QLD 4029, Australia*

Complete contact information is available at: https://pubs.acs.org/10.1021/acsbiomaterials.0c01284

Notes

The authors declare no competing financial interest.

■ ACKNOWLEDGMENTS

A.R. is a recipient of the Australian Government Research Training Program Scholarship from The University of Queensland, Brisbane, Australia. The authors also thank Professor Andrew K. Whittaker of the Australian Institute for Bioengineering and Nanotechnology (AIBN), The University of Queensland, Brisbane, QLD 4072, Australia, for his support and access to specialized equipment, including the liquid CO_2 unit used in this research. T.K. acknowledges the support from the National Medical and Health Research Council of Australia for an Early Career Fellowship (GNT1143296), Australian Research Council for Discovery Project (DP200102723), and the University of New South Wales for support and Scientia Grant. A.P. acknowledges Career Development Fellowship NHMRC. All the authors also acknowledge support from the Centre of Microscopy and Microanalysis and the School of Pharmacy, University of Queensland.

■ REFERENCES

(1) O'Neill, J. J. Tackling a global health crisis: initial steps. 2015.

(2) Ndayishimiye, J.; Popat, A.; Blaskovich, M.; Falconer, J. R. Formulation technologies and advances for oral delivery of novel nitroimidazoles and antimicrobial peptides. *J. Controlled Release* **2020**, *324*, 728−749.

(3) Xiong, M.-H.; Bao, Y.; Yang, X.-Z.; Zhu, Y.-H.; Wang, J. Delivery of antibiotics with polymeric particles. *Adv. Drug Delivery Rev.* **2014**, *78*, 63−76.

(4) *Meropenem trihydrate*; DRUG BANK: https://www.drugbank.ca/salts/DBSALT002823.

(5) Benet, L. Z.; Broccatelli, F.; Oprea, T. BDDCS applied to over 900 drugs. *AAPS J.* **2011**, *13* (4), 519−547.

(6) Odenholt, I.; Löwdin, E.; Cars, O. Infection, Comparative in vitro pharmacodynamics of BO-2727, Meropenem and imipenem against gram-positive and gram-negative bacteria. *Clin. Microbiol. Infect.* **1997**, *3* (1), 73−81.

(7) Prince, B. T.; McMahon, B. J.; Jain, M.; Peters, A. T. Meropenem tolerance in a patient with probable fulminant piperacillin-induced immune hemolytic anemia. *Journal of Allergy and Clinical immunology. In Practice* **2015**, *3* (3), 452−453.

(8) Santos Filho, L.; Eagye, K.; Kuti, J.; Nicolau, D. Addressing resistance evolution in Pseudomonas aeruginosa using pharmacodynamic modelling: application to Meropenem dosage and combination therapy. *Clin. Microbiol. Infect.* **2007**, *13* (6), 579−585.

(9) Baldwin, C. M.; Lyseng-Williamson, K. A.J.; Keam, S. Meropenem: A Review of its Use in the Treatment of Serious Bacterial Infections. *Drugs* **2008**, *68* (6), 803−838.

(10) Edwards, J. Meropenem: a microbiological overview. *J. Antimicrob. Chemother.* **1995**, *36* (suppl_A), 1−17.

(11) Mollá-Cantavella, S.; Ferriols-Lisart, R.; Torrecilla-Junyent, T.; Alós-Almiñana, M. Intravenous Meropenem stability in physiological saline at room temperature. *European Journal of Hospital Pharmacy* **2014**, *21* (4), 202−207.

(12) Manning, L.; Wright, C.; Ingram, P. R.; Whitmore, T. J.; Heath, C. H.; Manson, I.; Page-Sharp, M.; Salman, S.; Dyer, J.; Davis, T. M. Continuous infusions of Meropenem in ambulatory care: clinical efficacy, safety and stability. *PLoS One* **2014**, *9* (7), No. e102023.

(13) Craig, W. A. The pharmacology of Meropenem, a new carbapenem antibiotic. *Clin. Infect. Dis.* **1997**, *24* (Supplement_2), S266−S275.

(14) Pharmaceuticals, A. MERREM® IV (Meropenem for injection). 2016.

(15) Papp-Wallace, K. M.; Endimiani, A.; Taracila, M. A.; Bonomo, R. A. Carbapenems: past, present, and future. *Antimicrob. Agents Chemother.* **2011**, *55* (11), 4943−4960.

(16) Fawaz, S.; Barton, S.; Whitney, L.; Swinden, J.; Nabhani-Gebara, S. Stability of Meropenem after reconstitution for administration by prolonged infusion. *Hosp. Pharm.* **2019**, *54* (3), 190−196.
(17) Talaczyńska, A.; Lewandowska, K.; Garbacki, P.; Zalewski, P.; Skibiński, R.; Miklaszewski, A.; Mizera, M.; Cielecka-Piontek, J. Solid-state stability studies of crystal form of tebipenem. *Drug Dev. Ind. Pharm.* **2016**, *42* (2), 238−244.
(18) Cielecka-Piontek, J.; Paczkowska, M.; Lewandowska, K.; Barszcz, B.; Zalewski, P.; Garbacki, P. Solid-state stability study of Meropenem-solutions based on spectrophotometric analysis. *Chem. Cent. J.* **2013**, *7* (1), 98.
(19) Jaruratanasirikul, S.; Sriwiriyajan, S. Stability of Meropenem in normal saline solution after storage at room temperature. *Southeast Asian J. Trop. Med. Public Health* **2003**, *34* (3), 627−629.
(20) Saito, T.; Sawazaki, R.; Ujiie, K.; Oda, M.; Saitoh, H. Possible factors involved in oral inactivity of Meropenem, a carbapenem antibiotic. *Pharmacol. Pharm.* **2012**, *3*, 6.
(21) Singh, S. B.; Rindgen, D.; Bradley, P.; Suzuki, T.; Wang, N.; Wu, H.; Zhang, B.; Wang, L.; Ji, C.; Yu, H. Design, Synthesis, Structure-Function Relationship, Bioconversion, and Pharmacokinetic Evaluation of Ertapenem Prodrugs. *J. Med. Chem.* **2014**, *57* (20), 8421−8444.
(22) Teitelbaum, A. M.; Meissner, A.; Harding, R. A.; Wong, C. A.; Aldrich, C. C.; Remmel, R. P. Synthesis, pH-dependent, and plasma stability of Meropenem prodrugs for potential use against drug-resistant tuberculosis. *Bioorg. Med. Chem.* **2013**, *21* (17), 5605−5617.
(23) Cielecka-Piontek, J.; Zalewski, P.; Paczkowska, M. The chromatographic approach to kinetic studies of tebipenem pivoxil. *J. Chromatogr. Sci.* **2015**, *53* (2), 325−330.
(24) Teitelbaum, A. M.; Meissner, A.; Harding, R. A.; Wong, C. A.; Aldrich, C. C.; Remmel, R. P. J. B.; Chemistry, M. Synthesis, pH-dependent, and plasma stability of Meropenem prodrugs for potential use against drug-resistant tuberculosis. *Bioorg. Med. Chem.* **2013**, *21* (17), 5605−5617.
(25) Reis, C. P.; Martinho, N.; Damgé, C. Nanotechnology for Oral Drug Delivery and Targeting:Nano-Engineering Strategies Nanomedicines against Severe Diseases. *In Nanotechnology Drug Delivery* **2016**, *2*, 20.
(26) Martins, J. P.; das Neves, J.; de la Fuente, M.; Celia, C.; Florindo, H.; Günday-Türeli, N.; Popat, A.; Santos, J. L.; Sousa, F.; Schmid, R. The solid progress of nanomedicine. *Drug Delivery Transl. Res.* **2020**, *10*, 1−4.
(27) Raza, A.; Sun, H.; Bano, S.; Zhao, Y.; Xu, X.; Tang, J. Preparation, characterization, and in vitro anti-inflammatory evaluation of novel water soluble kamebakaurin/hydroxypropyl-β-cyclodextrin inclusion complex. *J. Mol. Struct.* **2017**, *1130*, 319−326.
(28) Raza, A.; Sime, F. B.; Cabot, P. J.; Maqbool, F.; Roberts, J. A.; Falconer, J. R. Solid nanoparticles for oral antimicrobial drug delivery: A review. *Drug Discovery Today* **2019**, *24* (3), 858−866.
(29) Drulis-Kawa, Z.; Gubernator, J.; Dorotkiewicz-Jach, A.; Doroszkiewicz, W.; Kozubek, A. In vitro antimicrobial activity of liposomal Meropenem against Pseudomonas aeruginosa strains. *Int. J. Pharm.* **2006**, *315* (1−2), 59−66.
(30) Khanum, R.; Qureshi, M.; Mohandas, K. Antibiofilm Potential of Meropenem-Loaded Poly (ε-Caprolactone) Nano particles Against Klebsiella pneumoniae. *Int. J. Pharm. Clin. Res.* **2016**, *8*, 1343−1350.
(31) Nandakumar, V.; Geetha, V.; Chittaranjan, S.; Doble, M. High glycolic poly (DL lactic co glycolic acid) nanoparticles for controlled release of Meropenem. *Biomed. Pharmacother.* **2013**, *67* (5), 431−436.
(32) Mhango, E. K.; Kalhapure, R. S.; Jadhav, M.; Sonawane, S. J.; Mocktar, C.; Vepuri, S.; Soliman, M.; Govender, T. Preparation and optimization of Meropenem-loaded solid lipid nanoparticles: in vitro evaluation and molecular modeling. *AAPS PharmSciTech* **2017**, *18* (6), 2011−2025.
(33) Abeer, M. M.; Rewatkar, P.; Qu, Z.; Talekar, M.; Kleitz, F.; Schmid, R.; Lindén, M.; Kumeria, T.; Popat, A. Silica nanoparticles: A promising platform for enhanced oral delivery of macromolecules. *J. Controlled Release* **2020**, *326*, 544−555.
(34) Chaudhary, Z.; Subramaniam, S.; Khan, G. M.; Abeer, M. M.; Qu, Z.; Janjua, T.; Kumeria, T.; Batra, J.; Popat, A. Encapsulation and controlled release of resveratrol within functionalized mesoporous silica nanoparticles for prostate cancer therapy. *Front. Bioeng. Biotechnol.* **2019**, *7*, 225.
(35) Juère, E.; Del Favero, G.; Masse, F.; Marko, D.; Popat, A.; Florek, J.; Caillard, R.; Kleitz, F. Gastro-protective protein-silica nanoparticles formulation for oral drug delivery: In vitro release, cytotoxicity and mitochondrial activity. *Eur. J. Pharm. Biopharm.* **2020**, *151*, 171−180.
(36) Xu, C.; Cao, Y.; Lei, C.; Li, Z.; Kumeria, T.; Meka, A. K.; Xu, J.; Liu, J.; Yan, C.; Luo, L. Polymer-Mesoporous Silica Nanoparticle Core-Shell Nanofibers as a Dual-Drug-Delivery System for Guided Tissue Regeneration. *ACS Applied Nano Materials* **2020**, *3* (2), 1457−1467.
(37) Meka, A. K.; Jenkins, L. J.; Dàvalos-Salas, M.; Pujara, N.; Wong, K. Y.; Kumeria, T.; Mariadason, J. M.; Popat, A. Enhanced solubility, permeability and anticancer activity of vorinostat using tailored mesoporous silica nanoparticles. *Pharmaceutics* **2018**, *10* (4), 283.
(38) Abeer, M. M.; Meka, A. K.; Pujara, N.; Kumeria, T.; Strounina, E.; Nunes, R.; Costa, A.; Sarmento, B.; Hasnain, S. Z.; Ross, B.; Popat, A. Rationally designed dendritic silica nanoparticles for oral delivery of exenatide. *Pharmaceutics* **2019**, *11* (8), 418.
(39) Ghaferi, M.; Koohi Moftakhari Esfahani, M.; Raza, A.; Al Harthi, S.; Ebrahimi Shahmabadi, H.; Alavi, S. E. Mesoporous silica nanoparticles: synthesis methods and their therapeutic use-recent advances. *J. Drug Targeting* **2020**, 1−67.
(40) Raza, A.; Bano, S.; Xu, X.; Zhang, R. X.; Khalid, H.; Iqbal, F. M.; Xia, C.; Tang, J.; Ouyang, Z. Rutin-nickel complex: synthesis, characterization, antioxidant, DNA binding, and DNA cleavage activities. *Biol. Trace Elem. Res.* **2017**, *178* (1), 160−169.
(41) Ghaferi, M.; Amari, S.; Mohrir, B. V.; Raza, A.; Shahmabadi, H. E.; Alavi, S. E. Preparation, Characterization, and Evaluation of Cisplatin-Loaded Polybutylcyanoacrylate Nanoparticles with Improved In Vitro and In Vivo Anticancer Activities. *Pharmaceuticals* **2020**, *13* (3), 44.
(42) Raza, A.; Xu, X.; Xia, L.; Xia, C.; Tang, J.; Ouyang, Z. Quercetin-iron complex: synthesis, characterization, antioxidant, DNA binding, DNA cleavage, and antibacterial activity studies. *J. Fluoresc.* **2016**, *26* (6), 2023−2031.
(43) Raza, A.; Sime, F. B.; Cabot, P. J.; Maqbool, F.; Roberts, J. A.; Falconer, J. R. J. D. D. T. *Drug Discovery Today* **2019**, *24* (3), 858−866.
(44) Florek, J.; Caillard, R.; Kleitz, F. Evaluation of mesoporous silica nanoparticles for oral drug delivery-current status and perspective of MSNs drug carriers. *Nanoscale* **2017**, *9* (40), 15252−15277.
(45) Pourmortazavi, S. M.; Saghafi, Z.; Ehsani, A.; Yousefi, M. Application of supercritical fluids in cholesterol extraction from foodstuffs: a review. *J. Food Sci. Technol.* **2018**, *55* (8), 2813−2823.
(46) Kankala, R. K.; Zhang, Y. S.; Wang, S. B.; Lee, C. H.; Chen, A. Z. Supercritical fluid technology: An emphasis on drug delivery and related biomedical applications. *Adv. Healthcare Mater.* **2017**, *6* (16), 1700433.
(47) Djerafi, R.; Masmoudi, Y.; Crampon, C.; Meniai, A.; Badens, E. Supercritical anti-solvent precipitation of ethyl cellulose. *J. Supercrit. Fluids* **2015**, *105*, 92−98.
(48) Yoon, T. J.; Son, W.-S.; Park, H. J.; Seo, B.; Kim, T.; Lee, Y.-W. Tetracycline nanoparticles precipitation using supercritical and liquid CO2 as antisolvents. *J. Supercrit. Fluids* **2016**, *107*, 51−60.
(49) Pourjavadi, A.; Tehrani, Z. M. Mesoporous silica nanoparticles (MCM-41) coated PEGylated chitosan as a pH-responsive nanocarrier for triggered release of erythromycin. *Int. J. Polym. Mater.* **2014**, *63* (13), 692−697.
(50) Mohammadzadeh, R.; Baradaran, B.; Valizadeh, H.; Yousefi, B.; Zakeri-Milani, P. Reduced ABCB1 expression and activity in the presence of acrylic copolymers. *Adv. Pharm. Bull.* **2014**, *4* (3), 219.
(51) Popova, M.; Trendafilova, I.; Zgureva, D.; Kalvachev, Y.; Boycheva, S.; Tušar, N. N.; Szegedi, A. Polymer-coated mesoporous

silica nanoparticles for controlled release of the prodrug sulfasalazine. *J. Drug Delivery Sci. Technol.* **2018**, *44*, 415−420.
(52) Abbaraju, P. L.; Kumar Meka, A.; Jambhrunkar, S.; Zhang, J.; Xu, C.; Popat, A.; Yu, C. Floating tablets from mesoporous silica nanoparticles. *J. Mater. Chem. B* **2014**, *2* (47), 8298−8302.
(53) Bouchoucha, M.; Cote, M.-F. C.; Gaudreault, R.; Fortin, M.-A.; Kleitz, F. Size-controlled functionalized mesoporous silica nanoparticles for tunable drug release and enhanced anti-tumoral activity. *Chem. Mater.* **2016**, *28* (12), 4243−4258.
(54) Kecht, J.; Schlossbauer, A.; Bein, T. Selective functionalization of the outer and inner surfaces in mesoporous silica nanoparticles. *Chem. Mater.* **2008**, *20* (23), 7207−7214.
(55) Mendez, A. S.; Steppe, M.; Schapoval, E. E. Validation of HPLC and UV spectrophotometric methods for the determination of Meropenem in pharmaceutical dosage form. *J. Pharm. Biomed. Anal.* **2003**, *33* (5), 947−954.
(56) US Pharmacopeia Test Solution for Simulated Gastric Fluid. http://www.pharmacopeia.cn/v29240/usp29nf24s0_ris1s126.html.
(57) Kigen, G.; Edwards, G. Drug-transporter mediated interactions between anthelminthic and antiretroviral drugs across the Caco-2 cell monolayers. *BMC Pharmacol. Toxicol.* **2017**, *18* (1), 20.
(58) Liu, W.-D.; Shih, M.-C.; Chuang, Y.-C.; Wang, J.-T.; Sheng, W.-H. Comparative efficacy of doripenem versus Meropenem for hospital-acquired and ventilator-associated pneumonia. *Journal of Microbiology, Immunology and Infection* **2019**, *52* (5), 788−795.
(59) Balouiri, M.; Sadiki, M.; Ibnsouda, S. K. Methods for in vitro evaluating antimicrobial activity: A review. *J. Pharm. Anal.* **2016**, *6* (2), 71−79.
(60) Barry, A. L.; Craig, W. A.; Nadler, H.; Reller, L. B.; Sanders, C. C.; Swenson, J. M. Methods for determining bactericidal activity of antimicrobial agents: approved guideline. 1999, *19* (18).
(61) Juěre, E.; Florek, J.; Bouchoucha, M.; Jambhrunkar, S.; Wong, K. Y.; Popat, A.; Kleitz, F. In vitro dissolution, cellular membrane permeability, and anti-inflammatory response of resveratrol-encapsulated mesoporous silica nanoparticles. *Mol. Pharmaceutics* **2017**, *14* (12), 4431−4441.
(62) Faghihian, H.; Naghavi, M. Synthesis of Amine-Functionalized MCM-41 and MCM-48 for removal of heavy metal ions from aqueous solutions. *Sep. Sci. Technol.* **2014**, *49* (2), 214−220.
(63) Mahardika, I. B. P.; Trisunaryanti, W.; Triyono, T.; Wijaya, D. P.; Dewi, K. Transesterification of Used Cooking Oil Using CaO/MCM-41 Catalyst Synthesized from Lapindo Mud by Sonochemical Method. *Indones. J. Chem.* **2017**, *17*, 509−515.
(64) Sun, X.-Y.; Li, P.-Z.; Ai, B.; Wang, Y.-B. Surface modification of MCM-41 and its application in DNA adsorption. *Chin. Chem. Lett.* **2016**, *27* (1), 139−144.
(65) De Leo, V.; Di Gioia, S.; Milano, F.; Fini, P.; Comparelli, R.; Mancini, E.; Agostiano, A.; Conese, M.; Catucci, L. Eudragit S100 entrapped liposome for curcumin delivery: Anti-oxidative effect in Caco-2 cells. *Coatings* **2020**, *10* (2), 114.
(66) Nguyen, C. T.; Webb, R. I.; Lambert, L. K.; Strounina, E.; Lee, E. C.; Parat, M.-O.; McGuckin, M. A.; Popat, A.; Cabot, P. J.; Ross, B. P. Bifunctional succinylated ε-polylysine-coated mesoporous silica nanoparticles for pH-responsive and intracellular drug delivery targeting the colon. *ACS Appl. Mater. Interfaces* **2017**, *9* (11), 9470−9483.
(67) O'Connell, C. L.; Nooney, R.; McDonagh, C. Cyanine5-doped silica nanoparticles as ultra-bright immunospecific labels for model circulating tumour cells in flow cytometry and microscopy. *Biosens. Bioelectron.* **2017**, *91*, 190−198.
(68) Lian, Y.; Ding, L.-J.; Zhang, W.; Zhang, X.-A.; Zhang, Y.-L.; Lin, Z.-Z.; Wang, X.-D. Synthesis of highly stable cyanine-dye-doped silica nanoparticle for biological applications. *Methods Appl. Fluoresc.* **2018**, *6* (3), 034002.
(69) Czarnobaj, K.; Prokopowicz, M.; Sawicki, W. Formulation and in vitro characterization of bioactive mesoporous silica with doxorubicin and metronidazole intended for bone treatment and regeneration. *AAPS PharmSciTech* **2017**, *18* (8), 3163−3171.
(70) Meropenem trihydrate: Pub Chem. https://pubchem.ncbi.nlm.nih.gov/compound/Meropenem-trihydrate.
(71) Subudhi, M. B.; Jain, A.; Jain, A.; Hurkat, P.; Shilpi, S.; Gulbake, A.; Jain, S. K. Eudragit S100 coated citrus pectin nanoparticles for colon targeting of 5-fluorouracil. *Materials* **2015**, *8* (3), 832−849.
(72) Chaudhary, Z.; Khan, G. M.; Abeer, M. M.; Pujara, N.; Tse, B. W.-C.; McGuckin, M. A.; Popat, A.; Kumeria, T. Efficient photoacoustic imaging using indocyanine green (ICG) loaded functionalized mesoporous silica nanoparticles. *Biomater. Sci.* **2019**, *7* (12), 5002−5015.
(73) Artursson, P.; Palm, K.; Luthman, K. Caco-2 monolayers in experimental and theoretical predictions of drug transport. *Adv. Drug Delivery Rev.* **2001**, *46* (1−3), 27−43.
(74) Bergeon, J. A.; Ziora, Z. M.; Abdelrahim, A. S.; Pernevi, N. U.; Moss, A. R.; Toth, I. In vitro and in vivo evaluation of positively charged liposaccharide derivatives as oral absorption enhancers for the delivery of anionic drugs. *J. Pharm. Sci.* **2010**, *99* (5), 2333−2342.
(75) Garcia, A.; Macedo, M. H.; Azevedo, M. J.; Pestana, M.; Sarmento, B.; Sampaio-Maia, B. Effect of uremic state in intestine through a co-culture in vitro intestinal epithelial model. *Int. J. Pharm.* **2020**, *584*, 119450.
(76) Lamson, N. G.; Berger, A.; Fein, K. C.; Whitehead, K. A. Anionic nanoparticles enable the oral delivery of proteins by enhancing intestinal permeability. *Nature Biomedical Engineering* **2020**, *4* (1), 84−96.
(77) Gao, Y.; Chen, Y.; Ji, X.; He, X.; Yin, Q.; Zhang, Z.; Shi, J.; Li, Y. Controlled intracellular release of doxorubicin in multidrug-resistant cancer cells by tuning the shell-pore sizes of mesoporous silica nanoparticles. *ACS Nano* **2011**, *5* (12), 9788−9798.
(78) Zhou, Y.; Quan, G.; Wu, Q.; Zhang, X.; Niu, B.; Wu, B.; Huang, Y.; Pan, X.; Wu, C. Mesoporous silica nanoparticles for drug and gene delivery. *Acta Pharm. Sin. B* **2018**, *8* (2), 165−177.
(79) Shen, J.; He, Q.; Gao, Y.; Shi, J.; Li, Y. Mesoporous silica nanoparticles loading doxorubicin reverse multidrug resistance: performance and mechanism. *Nanoscale* **2011**, *3* (10), 4314−4322.
(80) Huang, I.-P.; Sun, S.-P.; Cheng, S.-H.; Lee, C.-H.; Wu, C.-Y.; Yang, C.-S.; Lo, L.-W.; Lai, Y.-K. Enhanced chemotherapy of cancer using pH-sensitive mesoporous silica nanoparticles to antagonize P-glycoprotein-mediated drug resistance. *Mol. Cancer Ther.* **2011**, *10* (5), 761−769.
(81) Raza, A.; Ngieng, S. C.; Sime, F. B.; Cabot, P. J.; Roberts, J. A.; Popat, A.; Kumeria, T.; Falconer, J. R. Oral Meropenem for superbugs: challenges and opportunities. *Drug Discovery Today* 2020.
(82) Nassar, T.; Rom, A.; Nyska, A.; Benita, S. Novel double coated nanocapsules for intestinal delivery and enhanced oral bioavailability of tacrolimus, a P-gp substrate drug. *J. Controlled Release* **2009**, *133* (1), 77−84.
(83) Karolewicz, B. A review of polymers as multifunctional excipients in drug dosage form technology. *Saudi Pharm. J.* **2016**, *24* (5), 525−536.
(84) Nassar, T.; Rom, A.; Nyska, A.; Benita, S. A novel nanocapsule based delivery system approach to enhance intestinal transport and absorption of lipophilic P-glycoprotein substrate drugs. *Pharm. Res.* **2008**, *25*, 2019−2029.
(85) Gurjar, R.; Chan, C. Y.; Curley, P.; Sharp, J.; Chiong, J.; Rannard, S.; Siccardi, M.; Owen, A. Inhibitory effects of commonly used excipients on P-glycoprotein in vitro. *Mol. Pharmaceutics* **2018**, *15* (11), 4835−4842.
(86) European Committee on AntimicrobialSusceptibility Testing. http://www.eucast.org/fileadmin/src/media/PDFs/EUCAST_files/QC/v_10.0_EUCAST_QC_tables_routine_and_extended_QC.pdf. 2020.
(87) European Committee on Antimicrobial Susceptibility Testing. http://www.eucast.org/fileadmin/src/media/PDFs/EUCAST_files/Disk_test_documents/EUCAST_QC_Tables_V1.1.pdf. 2010.
(88) Weinstein, M. P.; Lewis, J. S. The Clinical and Laboratory Standards Institute Subcommittee on Antimicrobial Susceptibility Testing: Background, Organization, Functions, and Processes. *J. Clin. Microbiol.* **2020**, *58* (3), 1−7.

https://dx.doi.org/10.1021/acsbiomaterials.0c01284
ACS Biomater. Sci. Eng. 2021, 7, 1836−1853

(89) Azad, M. A.; Finnin, B. A.; Poudyal, A.; Davis, K.; Li, J.; Hill, P. A.; Nation, R. L.; Velkov, T.; Li, J. Polymyxin B induces apoptosis in kidney proximal tubular cells. *Antimicrob. Agents Chemother.* **2013**, *57* (9), 4329−4335.

https://dx.doi.org/10.1021/acsbiomaterials.0c01284
ACS Biomater. Sci. Eng. 2021, 7, 1836−1853